

**VIBRATION POWER MEASUREMENT USING
A PLATE AS A REVERBERANT STRUCTURE**

by

Thomas Grant Irvine

**A Thesis Presented in Partial Fulfillment of the
Requirements for the Degree Master of Science**

ARIZONA STATE UNIVERSITY

May 1987

**VIBRATION POWER MEASUREMENT USING
A PLATE AS A REVERBERANT STRUCTURE**

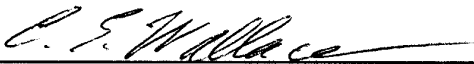
by

Thomas Grant Irvine

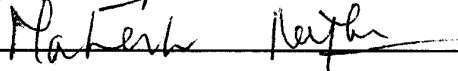
Has Been Approved

March 1987

APPROVED:


_____, Chairperson





Supervisory Committee

ACCEPTED:



Department Chairperson



Dean, Graduate College

ABSTRACT

A theoretical and experimental foundation is established for a reverberant field method of measuring the vibrational power input from a source into an adjoining structure. This method is analogous to the reverberant chamber method of measuring the sound power output of an acoustic source. The reverberant field method is carried out by mounting the vibration source on a referee structure which has been calibrated in terms of its frequency band average loss factors and its mechanical point impedance. The spatial average of the mean square velocity in the reverberant field is measured in order to calculate the power input from the source. The power is calculated by means of the reverberant field theory.

In this thesis an aluminum plate is used as a referee structure. The loss factors are measured by the multi-degree-of-freedom complex exponential method. An electromagnetic shaker is mounted to the plate via an impedance head to simulate a source. The power input in the 0-4000 Hz frequency range is measured by means of the reverberant field method and by means of the impedance head signals. The results of the two methods show reasonable agreement and thereby provide experimental validation of the reverberant field method.

ACKNOWLEDGEMENTS

I express sincere gratitude to Dr. C. E. Wallace. His patience and guidance were essential to the completion of this thesis. He has led me on a fascinating journey into the realm of vibrational power flow phenomenon.

I thank Dr. Harold Nelson, who helped me obtain assistantships and financial aid. I also appreciate Dr. Mahesh Rajan, who served on my supervisory committee along with Drs. Nelson and Wallace.

During my stay at Arizona State University, I have had the opportunity to share office space with students from India and Taiwan. I appreciate their friendship and have enjoyed learning about their cultures.

Finally, I gratefully acknowledge Garrett Fluid Systems Division for funding portions of this research and Gordon Whelpley for his consultation.

TABLE OF CONTENTS

	Page
LIST OF FIGURES	vii
LIST OF TABLES	ix
CHAPTER	
1. INTRODUCTION	1
1.1 Objective	1
1.2 Background Literature Review	1
1.3 Reverberant Sound Chamber Analogy	5
1.4 Current Approach	6
2. POWER MEASUREMENT THEORY	9
2.1 Introduction	9
2.2 Impedance Head Method	10
2.3 Reverberant Field Method	14
2.4 Mechanical Impedance Method	21
3. ENERGY LOSS MECHANISMS	23
3.1 Introduction	23
3.2 Structural Damping	23
3.3 Radiation Loss	27
4. DAMPING MEASUREMENT	30
4.1 Introduction	30
4.2 Decay Method	30
4.3 MDOF Complex Exponential Method	34
5. EXPERIMENTAL RESULTS	36

6. CONCLUSION	64
6.1 Loss Factors	64
6.2 Direct and Reverberant Field Considerations	65
6.3 Input Power Results	66
6.4 Point Impedance	66
6.5 Recommendations	67
BIBLIOGRAPHY	70
APPENDIX	
A. IMPEDANCE HEAD POWER PROGRAM	71
B. MEAN SQUARE VELOCITY PROGRAM	75
C. POINT IMPEDANCE PROGRAM	79
D. DERIVATION OF THE MDOF COMPLEX EXPONENTIAL METHOD	83

LIST OF FIGURES

Figure	Page
2.1 PLATE BOUNDARY LENGTH	16
3.1 ENERGY DISSIPATION	24
3.2 ACOUSTIC RADIATION FROM A FLEXURAL WAVE	28
4.1 TYPICAL DECAY CURVE	33
5.1 PLATE AND SHAKER	38
5.2 EQUIPMENT SET-UP	39
5.3 INDIVIDUAL LOSS FACTORS FOR THE 1/4 IN THICK PLATE	41
5.4 INDIVIDUAL LOSS FACTORS FOR THE 1/2 IN THICK PLATE	42
5.5 POWER INPUT INTO 1/4 IN THICK PLATE, 2.0 V CASE	43
5.6 POWER INPUT INTO 1/4 IN THICK PLATE, 2.5 V CASE	44
5.7 POWER INPUT INTO 1/4 IN THICK PLATE, 3.0 V CASE	45
5.8 POWER INPUT INTO 1/4 IN THICK PLATE, 3.5 V CASE	46
5.9 POWER INPUT INTO 1/4 IN THICK PLATE, 4.0 V CASE	47
5.10 POWER INPUT INTO 1/4 IN THICK PLATE, 4.5 V CASE	48
5.11 POWER INPUT INTO 1/2 IN THICK PLATE, 2.0 V CASE	49
5.12 POWER INPUT INTO 1/2 IN THICK PLATE, 2.5 V CASE	50
5.13 POWER INPUT INTO 1/2 IN THICK PLATE, 3.0 V CASE	51
5.14 POWER INPUT INTO 1/2 IN THICK PLATE, 3.5 V CASE	52
5.15 POWER INPUT INTO 1/2 IN THICK PLATE, 4.0 V CASE	53
5.16 POWER INPUT INTO 1/2 IN THICK PLATE, 4.5 V CASE	54
5.17 AVERAGE ERROR FOR 1/4 IN THICK PLATE	55

CHAPTER 1

INTRODUCTION

1.1 Objective

When two or more resonant structures are joined together, the vibrational energy flow between them can be estimated by a method called Statistical Energy Analysis (SEA). This method uses statistical techniques to average the behavior of individual modes in frequency bands. The mean energy flow between subsystems in a given frequency band can thus be analyzed.

SEA can be used to model systems of structures including beams, plates, cylinders, circuit boards, etc. In order to carry out this analysis, certain properties of each structure must be known. These include the mechanical point impedance, modal density, and loss factor for each structure. The coupling loss factor between each pair of structures must also be known.

In addition, the amount of energy input to each structure by external sources must also be determined in order to model the energy flow within the system. This external excitation could be caused, for example, by a turbulent boundary layer, acoustic radiation, or by direct contact with a mechanical vibration source. This thesis deals with the case of power input from an external mechanical device into an adjoining structure. A method is developed for measuring the power input from the device to the structure. This method is analogous to the reverberant chamber method of measuring acoustic power and is based upon previous SEA research.

1.2 Background Literature Review

The development of SEA can be traced back to work done by Lyon, Maidanik, and Smith in the 1960's. Lyon and Maidanik [1] studied the power flow between two lightly

coupled linear resonators excited by white noise sources. They found that the power flow was proportional to the difference in uncoupled energies of the systems, and that the power always flowed from the system with higher modal energy to the system with lower modal energy. Modal energy is defined as

$$E_m = [E(\Delta\omega)]/[n(\omega)\Delta\omega] \quad (1.1)$$

where $E(\Delta\omega)$ is the total energy in the system in frequency band $\Delta\omega$, and $n(\omega)$ is the modal density in the band.

The other contribution to the early development of SEA came from Smith [2], who studied the response of the structural modes of a linear resonator to excitation from a diffuse sound field. Lyon and Smith presented their combined research in a NASA report [3]. This report was the first comprehensive treatment of SEA.

After these publications a wealth of SEA literature appeared. This research was divided along two lines. One line was the examination and clarification of the basic SEA assumptions. The other line was the application of SEA to a wide variety of engineering problems.

In 1975 Lyon [4] wrote an SEA textbook which summarized these developments. In this text Lyon presented a derivation of the reverberant field method for calculation of the power input Π_{in} from a device to an adjoining structure. This derivation yields the formula

$$\Pi_{in} = M\omega\eta\langle v^2 \rangle \quad (1.2)$$

where M is the mass of the plate, ω is the band center frequency, η is the average loss factor, and $\langle v^2 \rangle$ is the spatial average of the mean square velocity in the reverberant field. Equation (1.2) is referred to as the reverberant field energy method. Lyon suggested that this method could be used to calculate the loss factors provided the input power was known

or to calculate the input power provided the loss factors were known. Equation (1.2) can be derived either by taking a wave propagation approach or by using an eigenfunction expansion in the bending-wave equation, which is the governing differential equation of motion. Lyon presented both of these approaches in his text.

In recent years Clarkson and others have devoted attention to the problem of determining loss factors. Clarkson and Pope [5,6] used the reverberant field energy method and the decay method to measure the loss factors on a cylinder in the frequency range 0-2000 Hz. The decay method is a method by which loss factors can be obtained from reverberation times. Clarkson and Pope found that the energy method gave values which were approximately an order of magnitude greater than the corresponding values obtained from the decay tests. They concluded that the decays were dominated by the mode having the lowest damping in each frequency band. They thus reasoned that the energy method should give a more accurate average value than the decay method.

Clarkson, Ranky, and Brown [7,8] examined the discrepancy between the energy and decay methods more closely. They used each method to measure the loss factors on a flat plate in the frequency range 0-2000 Hz. They found that the decay method results agreed with the energy method results for bands in which the modes all have similar loss factors. They also used the half power bandwidth method to determine the loss factors for individual modes in the 200-300 Hz frequency range. They found that in this frequency range the individual loss factors were all closely scattered about the average loss factor obtained from the energy method.

Dimitriadis [9] used the half power bandwidth method to measure loss factors in an L-shaped plate in the frequency range 0-7000 Hz. He found that 40% of the modes in this range were distinct enough to be measured by this method. He stated that this percentage was adequate enough since he saw no reason for the overlapping modes to be more or less damped than the well separated ones. Dimitriadis also measured the loss factors by the

decay method and found that the results from the two methods agreed reasonably well. He then used these loss factors in conjunction with SEA theory to determine the coupling loss factors between the two plates.

Wallace [10] derived expressions for the direct field energy density and the reverberant field energy density in a thin plate. The direct field energy density ϵ_d is

$$\epsilon_d = \frac{\Pi_{in} Q_\theta \exp[-\omega \eta_a r / c_g]}{2\pi r c_g} \quad (1.3)$$

where Q_θ is the directivity of the power flow, η_a is the distributed loss factor, r is the radius from the source, and c_g is the group velocity of the wave energy. The reverberant field energy density ϵ_r is

$$\epsilon_r = \frac{\Pi_{in} (1 - \alpha) \exp[-\omega \eta_a \pi A / 2p c_g]}{p \alpha c_g / \pi + A \omega \eta_a} \quad (1.4)$$

where α is the average boundary absorption coefficient, A is the area of the plate, and p is the perimeter. The average boundary absorption coefficient is related to the boundary loss factor η_L by

$$\alpha = \pi \omega A \eta_L / p c_g \quad (1.5)$$

The loss factor used in equation (1.2) is a sum of the distributed and boundary loss factors, $\eta = \eta_a + \eta_L$. Wallace thus showed that the direct field energy density could be compared to the reverberant field energy density at a given radius from the source provided the distributed and boundary loss factors are known. This comparison is important because

equation (1.2) was derived assuming that direct field strength is negligible compared to the reverberant field strength in the regions where the velocity is measured.

1.3 Reverberant Sound Chamber Analogy

This thesis also draws upon the reverberant chamber method of determining acoustic power output. A continuous sound source in a room produces two sound fields. One is the direct sound field, or direct arrival from the source. The other field, the reverberant field, is produced by the reflections from the surfaces of the room. In a reverberant sound chamber the boundaries are hard, and the total sound absorption is correspondingly small. The reverberant field thus dominates over the entire room volume with the exception of a small region around the source. The power output Π of a source can thus be calculated from

$$\Pi = aP_r^2/4\rho_0c \quad (1.6)$$

where a is the total sound absorption in the room, P_r is the effective acoustic pressure amplitude, and ρ_0c is the characteristic impedance of the air. Thus by calibrating a room in terms of its total sound absorption, the power output of a source can be determined by measuring the mean square pressure at points away from the source.

The method for measuring the vibrational power input from a device to a structure developed in this thesis is analogous to the reverberant chamber method for acoustic power measurement. In place of a reverberant chamber, an aluminum plate is used as a referee structure. In place of the total sound absorption in the room, the total loss factor of the plate is required. Whereas the mean square pressure was measured in the reverberation chamber, the mean square acceleration in the reverberant field of the plate is measured. The

corresponding mean square velocity values are calculated from the acceleration values according to

$$\langle v^2 \rangle = \frac{\langle a^2 \rangle}{(j\omega)^2} \quad (1.7)$$

The vibrational power input from the device to the plate can then be found from equation (1.2).

1.4 Current Approach

This thesis attempts to obtain valid results for more general cases than those presented by previous researchers in this field. Clarkson and others have shown that the energy method gives loss factors which agree reasonably well with those obtained by the decay method for bands in which the individual modes each have similar loss factors. They have also shown cases where the individual loss factors obtained from the half power bandwidth method were closely scattered about the average value obtained from the energy method. They have thus made an experimental verification of the reverberant field energy method for these cases.

Neither the decay method nor the half power bandwidth method is completely reliable for more general cases. The loss factors of individual modes in a structure can vary significantly within a single frequency band. In such cases the decay is dominated by the lowest damped mode in the band. The slope of the decay thus yields a loss factor which is much lower than the average value.

Furthermore, there are a number of cases where the half power bandwidth method and other single-degree-of-freedom (SDOF) techniques are inappropriate. The particular cases which demand a more elaborate treatment than that afforded by the SDOF concept are

those with closely-spaced modes. Systems with closely-spaced modes are those in which the natural frequencies are very closely spaced, or which have relatively heavy damping, or both. In these cases, severe modal overlapping will appear in the frequency response functions. For systems with extremely light damping, on the other hand, the resolution limitations of spectrum analyzers might cause the height of the peaks to be displayed on the low side and thus lead to an overestimate of the damping. For these cases accurate measurements at resonance are also difficult to obtain by an SDOF technique. A structure may even have its critical frequency in the frequency range of interest. The critical frequency is the frequency at which the phase speed of the flexural waves in the plate equals the speed of sound in the air. Near this frequency the damping increases sharply due to acoustic radiation.

These difficulties can be overcome to some extent by using a multi-degree-of-freedom (MDOF) method. MDOF methods are multi-mode curve-fitting extensions of SDOF methods. MDOF methods are also well-suited for measuring lightly damped modes. Ewins [11] gives a thorough description of these methods in his book.

The MDOF complex exponential method is used in this thesis to determine the loss factors for two aluminum plates in the 0-4000 Hz frequency range. An electromagnetic shaker is attached to each plate via an impedance head. The shaker and impedance head combination is considered to represent an external vibration device. The power flow from the shaker is measured by the force and acceleration signals from the impedance head. The spatial average of the mean square acceleration in the reverberant field is then measured. The corresponding velocity values are calculated from equation (1.7). The power input is then calculated from the loss factors and the mean square velocities in the reverberant field according to equation (1.2). The reverberant field results are then compared to the impedance head results in order to check the agreement and evaluate the validity of the reverberant field power method. This effort is made in order to demonstrate the validity of

the impedance head method for calibrating referee structures and to further establish the reverberant field energy method as a reliable method for determining the power input from an external device into an adjoining structure.

CHAPTER 2

POWER MEASUREMENT THEORY

2.1 Introduction

There are three basic approaches to determining the power input from a device to an adjoining structure: the impedance head method, the reverberant field method, and the mechanical impedance method. This chapter presents derivations of the first two methods and a brief discussion of the third.

The first method is the impedance head method. An impedance head is a transducer which has one piezoelectric crystal to measure the force input and another to measure the acceleration at the point where the force is applied. The analog signals from the impedance head can be fed into an analog-to-digital converter (ADC) and then into a computer which has the capability of performing Fourier transformations. The power input can then be obtained from the Fourier transforms of the force and acceleration signals by the method outlined in section 2.2.

The second method is the reverberant field power method. This method determines the steady state power lost through the dissipation and radiation of energy from the reverberant field. The acceleration in the reverberant field can be measured with an accelerometer and processed by the ADC. The Fourier transform of this signal can then be integrated according to equation (1.7) in order to determine the mean square velocity in the reverberant field. The power input can then be determined from the mean square velocity and the loss factors by equation (1.2). A derivation of this reverberant field method is given in section 2.3.

The third method is the mechanical impedance method. This method is actually an equivalent form of the impedance head method. Although the mechanical impedance

method was not used directly in this thesis, it is outlined in section 2.4 in order to show an important relationship between power input and mechanical impedance.

2.2 Impedance Head Method

The following derivation shows how input power can be determined from the force and acceleration signals from an impedance head. This derivation is similiar to one made by Fahy [12,13].

Power is generally expressed as the dot product of force and velocity. For a random force input the mean power is given by

$$\Pi_{in} = \lim_{T \rightarrow \infty} \frac{1}{T} \int_0^T f(t)v(t) dt \quad (2.1)$$

Assuming that force and velocity are stationary functions of time, their cross-correlation function is defined as

$$R_{FV}(\tau) = \lim_{T \rightarrow \infty} \frac{1}{T} \int_0^T f(t)v(t + \tau) dt \quad (2.2)$$

For zero time delay the cross-correlation function is

$$R_{FV}(0) = \lim_{T \rightarrow \infty} \frac{1}{T} \int_0^T f(t)v(t) dt \quad (2.3)$$

Thus, from equations (2.1) and (2.3), the input power is equal to the zero time delay cross-correlation of force and velocity

$$\Pi_{in} = R_{FV}(0) \quad (2.4)$$

Now assume that the velocity $v(t)$ can be expressed as a harmonic function

$$v(t) = v_0 \exp[-j\omega t] \quad (2.5a)$$

The acceleration $a(t)$ is thus

$$a(t) = -j\omega v_0 \exp[-j\omega t] = -j\omega v(t) \quad (2.5b)$$

The Fourier transform of the velocity $V(\omega)$ is thus related to the Fourier transform of the acceleration $A(\omega)$ by the relation

$$V(\omega) = \frac{j}{\omega} A(\omega) \quad (2.5c)$$

The cross-spectral density function of force and velocity G_{FV} is thus assumed to be related to the cross-spectral density function of force and acceleration G_{FA} by

$$G_{FV}(\omega) = \frac{j}{\omega} G_{FA}(\omega) \quad (2.5d)$$

The cross-correlation function is the inverse Fourier transform of the cross-spectral density function.

$$R_{FV}(\tau) = \int_{-\infty}^{\infty} G_{FV}(\omega) \exp(j\omega\tau) d\omega \quad (2.6)$$

Substituting equation (2.5d) into (2.6) yields

$$R_{FV}(\tau) = j \int_{-\infty}^{\infty} \frac{G_{FA}(\omega) \exp(j\omega\tau)}{\omega} d\omega \quad (2.7)$$

If $G_{FA}(\omega)$ is written as $C + j Q$, then

$$\begin{aligned} R_{FV}(\tau) = & - \int_{-\infty}^{\infty} \left[\frac{Q \cos \omega\tau + C \sin \omega\tau}{\omega} \right] d\omega \\ & + j \int_{-\infty}^{\infty} \left[\frac{C \cos \omega\tau - Q \sin \omega\tau}{\omega} \right] d\omega \end{aligned} \quad (2.8)$$

The cross-correlation function is a real function. Thus, the second integral in equation (2.8) is equal to zero. For a zero time delay, equation (2.8) simplifies to

$$R_{FV}(0) = - \int_{-\infty}^{\infty} \frac{Q}{\omega} d\omega \quad (2.9)$$

Substituting equation (2.9) into (2.4) yields

$$\Pi_{in} = - \int_{-\infty}^{\infty} \frac{Q}{\omega} d\omega \quad (2.10)$$

Now let $Y(f)$ be an equivalent one-sided spectral density function such that

$$Y(f) df = 2Q(\omega) d\omega \quad (2.11a)$$

Equation (2.10) may be written as

$$\Pi_{in} = - \frac{1}{2\pi} \int_0^{\infty} \frac{Y}{f} df \quad (2.11b)$$

To determine the power input in a particular frequency band (f_1, f_2) , equation (2.11b) may be modified as

$$\Pi_{\Delta f} = - \frac{1}{2\pi} \int_{f_1}^{f_2} \frac{Y}{f} df \quad (2.12)$$

Thus, the power input can be obtained from Y , the imaginary component of the one-sided cross-spectral density of force and acceleration.

For the purpose of this research, a GenRad 2510 Micromodal Analyzer was used to convert and process the force and acceleration signals. This computer has the capability of determining the Fourier transforms and the cross-correlation of the two input signals. A program was written in Time Series Language (TSL) as part of this thesis to utilize these capabilities to carry out the power calculation according to equation (2.12). A listing of this program is given in Appendix A.

2.3 Reverberant Field Method

The input power of a source can be derived as a function of the loss factor and the spatial average of the mean square velocity in the reverberant field. This derivation can be carried out by using an eigenfunction expansion in the bending-wave equation, which is the governing differential equation of motion. Cremer and Heckl [14] have used this approach in their textbook. The derivation can also be made by a wave propagation approach. The following derivation takes the wave propagation approach and is similar to derivations made by Lyon [4] and Wallace [10].

Assuming that the reverberant field is incoherent with the direct field, the total mean square velocity v^2 is the sum of the mean square velocity in the direct field v_D^2 and the mean square velocity in the reverberant field v_R^2 ,

$$v^2 = v_D^2 + v_R^2 \quad (2.13)$$

2.3.1 Direct Field

The energy flow for a point source radiates as a circular wave. The intensity relation yields the power of the waves Π as

$$\Pi(r) = Q_\theta \rho h c_g v_D^2 2\pi r \quad (2.14)$$

where Q_θ is the directivity of the power flow, ρ is the density of the plate, h is the plate thickness, c_g is the wave group velocity, and r is the distance from the source.

If there are no propagation losses, Π is equal to the power input by the source. If damping is present, the energy decay is given by

$$\Pi(r) = \Pi_{in} Q_\theta \exp[-\eta_a \omega r / c_g] \quad (2.15)$$

where Π_{in} is the power input by the source and η_a is the propagation loss factor.

Substituting (2.14) into (2.15) and solving for the mean square velocity in the direct field yields

$$v_D^2 = \frac{\Pi_{in} Q_\theta \exp[-\eta_a \omega r / c_g]}{2\pi r p h c_g} \quad (2.16)$$

In addition to interior losses, energy losses also occur at the boundaries. The power left in the reverberant field after a wave has undergone its first reflection is

$$\Pi = \Pi_{in} (1 - \alpha) \exp[-\omega \eta_a d / 2c_g] \quad (2.17)$$

where α is the fraction of energy lost during the reflection and d is the mean free path length. Note that

$$d = \pi A / p \quad (2.18)$$

where A is the plate area and p is the perimeter.

2.3.2 Reverberant Field

Now consider the relationship between the energy density and the energy flux across the boundaries of the plate. In Figure 2.1, let ΔL be an element of a boundary and dA an element of area in the plate at a distance r from ΔL , where r makes an angle θ with the normal to ΔL . The amount of energy that will strike ΔL by direct transmission is ϵdA attenuated by $2\pi r$ and multiplied by the projection of ΔL on the circle of radius r centered on dA ,

$$(\epsilon dA / 2\pi r) \Delta L \cos \theta$$

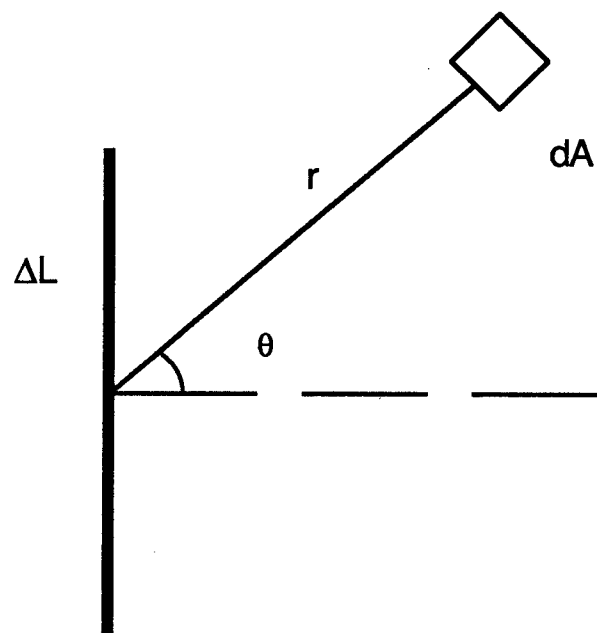


Figure 2.1 PLATE BOUNDARY LENGTH

This diagram is used in deriving an expression for the energy received by an element of boundary ΔL from an area dA which is at a distance r from ΔL , where r is at an angle θ from the normal to ΔL .

The energy contributed to ΔL by the entire half ring can be obtained by assuming that the energy arrives from any direction with equal probability. Integrating the half ring yields

$$dE = \int_{-\pi/2}^{\pi/2} \frac{\epsilon \Delta L}{2\pi r} \cos \theta r dr d\theta \quad (2.19)$$

Thus,

$$dE = \epsilon \Delta L dr / \pi \quad (2.20)$$

Since the wave group velocity is c_g ,

$$dr = c_g dt \quad (2.21)$$

Then, substituting equation (2.21) into (2.20) yields

$$\Delta \Pi = \frac{dE}{dt} = \epsilon \Delta L c_g / \pi \quad (2.22)$$

The power per unit boundary length is thus

$$\frac{d\Pi}{dL} = \epsilon c_g / \pi \quad (2.23)$$

Considering the average energy absorption a along the perimeter p , the total boundary absorption is αp . The rate at which energy is absorbed along the boundary is

$$\alpha p \frac{d\Pi}{dL} = \alpha p \epsilon c_g / \pi \quad (2.24)$$

Energy is also lost through damping in the interior of the plate. The rate of energy lost in the interior is $A\epsilon\eta_a\omega$. By conservation of energy, the power introduced into the plate must be equal to the sum of the power increase inside the plate and the power decrease by interior and boundary losses. Thus

$$\Pi = A \frac{d\epsilon}{dt} + [A\omega\eta_a + \alpha p c_g / \pi] \epsilon \quad (2.25)$$

Considering the steady state solution and solving for the energy density,

$$\epsilon = \frac{\Pi}{A\omega\eta_a + \alpha p c_g / \pi} \quad (2.26)$$

Substituting equation (2.17) into (2.26) to eliminate Π yields the energy density in the reverberant field

$$\epsilon_r = \frac{\Pi_{in} (1 - \alpha) \exp [-\omega\eta_a d]}{A\omega\eta_a + \alpha p c_g / \pi} \quad (2.27)$$

The kinetic energy in the reverberant field is

$$\epsilon_r = \rho A h v_R^2 \quad (2.28)$$

Thus, substituting equation (2.28) into (2.27) and solving for the mean square velocity in the reverberant field yields

$$v_R^2 = \frac{1}{\rho A h} \left[\frac{\Pi_{in} (1 - \alpha) \exp(-\omega \eta_a d / 2c_g)}{A \omega \eta_a + \alpha p c_g / \pi} \right] \quad (2.29)$$

Now define an equivalent loss factor η_L in terms of the average energy absorption along the perimeter

$$\eta_L = \frac{\alpha p c_g}{\pi \omega A} \quad (2.30)$$

Substituting equation (2.30) into (2.29) to eliminate α and replacing d by $\pi A/p$ yields

$$v_R^2 = \frac{\Pi_{in} [1 - (\eta_L \pi \omega A / p c_g)] \exp(-\omega \eta_a \pi A / 2 p c_g)}{\rho A h (\eta_a + \eta_L) \omega A} \quad (2.31)$$

2.3.3 Sum of Two Fields

Now substituting equations (2.31) and (2.16) into (2.13) gives

$$v^2 = \frac{\Pi_{in}}{\rho A h} \left[\frac{Q_\theta \exp(-\omega \eta_a r / c_g)}{2 \pi r} + \frac{1}{R} \right] \quad (2.32)$$

where

$$\frac{1}{R} = \frac{(1 - \pi\omega A\eta_L / pc_g) \exp(-\pi\omega A\eta_a / 2pc_g)}{A\omega(\eta_L + \eta_a)} \quad (2.33)$$

R is called the plate constant.

Now assume very small loss factors, $\eta_L \ll 1$ and $\eta_a \ll 1$. Taking the first two terms of the Taylor series expansion,

$$\exp[-\pi\omega A\eta_a / 2pc_g] \cong 1 - \pi\omega A\eta_a / 2pc_g \quad (2.34)$$

Substituting equation (2.34) into (2.33),

$$\frac{1}{R} \cong \frac{1 - (\pi\omega A / pc_g)(\eta_L + \eta_a / 2)}{A\omega(\eta_L + \eta_a)} \quad (2.35)$$

In reality, η_L and η_a cannot be measured separately. Thus, any damping measurement will determine their sum. Therefore, R can only be found if

$$(\pi\omega A / pc_g)(\eta_L + \eta_a / 2) \ll 1$$

Thus,

$$R \cong A\omega\eta / c_g \quad (2.36)$$

where $\eta = \eta_L + \eta_a$. Substituting equation (2.36) into (2.32) yields

$$v^2 \cong \frac{\Pi_{in}}{\rho hc_g} \left[\frac{Q_\theta \exp(-\omega\eta_a r / c_g)}{2\pi r} + \frac{1}{A\omega\eta} \right] \quad (2.37)$$

For a lightly damped plate, the reverberant field dominates over most of the plate except for a small region around the source. Thus, for the area outside of this region,

$$\frac{1}{A\omega\eta} \gg \frac{\exp(-\omega\eta_a r/c_g)}{2\pi r} \quad (2.38)$$

Using this assumption in equation (2.37) and solving for input power yields

$$\Pi_{in} \equiv M\eta\omega \langle v^2 \rangle \quad (2.39)$$

where M is the mass of the plate and $\langle \rangle$ denotes spatial average. Since the modal density is not infinite, a better representation of the energy in the reverberant field can be obtained by taking a spatial average of the velocity. A program was written in TSL in order to obtain a spatial average of the mean square velocity from the acceleration measurements. A listing of this program is given in Appendix B.

2.4 Mechanical Impedance Method

Mechanical impedance is defined as the complex ratio of the force acting on a specified area of a structure to the resulting linear velocity of that area. That is

$$Z = F / V$$

Clarkson [15] suggests a method for measuring the average power input by the relation

$$\Pi = f^2(t) \operatorname{Re}(1/Z) \quad (2.40)$$

where $\operatorname{Re}(1/Z)$ is the real component of the reciprocal of the impedance and $f^2(t)$ is the average of the mean square force.

Although this method was not used in this thesis, it is important because it shows the relationship between input power and impedance. The amount of power injected by a device to a structure is a function of the impedance of the structure itself. This relationship has an important implication for power measurement: the referee structure must have the same impedance as the actual structure upon which the device is to be permanently mounted in order to obtain accurate results. Thus, the impedance of the actual structure must be measured. Then a referee plate with the same impedance characteristics can be selected for the input power measurements. The measurements can then be carried out by mounting the device on the referee structure in the same manner that it is to be permanently mounted on the actual structure.

Formulae for the theoretical impedance of several special structures have been derived by Cremer and Heckl [14]. For an infinite plate the theoretical impedance is given by

$$Z = \frac{4}{\sqrt{3}} h^2 \rho c_L \quad (2.41)$$

where c_L is the propagation velocity of the longitudinal waves in the plate material. Equation (2.41) may also be used to approximate the impedance of large finite plates. Thus, for example, equation (2.41) could be used to determine the thickness h of a referee plate needed to match the impedance of the actual structure. The impedance of the referee plates should, nevertheless, be measured in order to verify that they have the desired impedance.

As part of this thesis, the impedance of the plates was measured. The results are given in Chapter V. In order to carry out these measurements, a computer program was written using TSL. A listing of this program is given in Appendix C.

CHAPTER 3

ENERGY LOSS MECHANISMS

3.1 Introduction

The loss factor η is defined as the fraction of energy lost per radian of oscillation. In order to use the plates as referee structures, they must be calibrated in terms of their loss factors. The loss factors of individual modes can be averaged arithmetically in order to obtain an average loss factor for each frequency band of interest.

The energy injected into the plate can be lost through two general mechanisms: dissipation and radiation. Dissipation mechanisms include internal structural damping and friction at the boundaries. The plates used in this thesis were suspended vertically by elastic cords in order to approximate free boundary conditions at all of the edges. Thus the energy losses at the boundaries were minimized. The radiation mechanism which is of major concern in this thesis is acoustic radiation. The loss factors measured in this thesis actually represent the combined effect of all of the energy loss mechanisms. Nevertheless, a consideration of the individual mechanisms is essential in order to understand the behavior of the plates. This chapter deals with the mechanisms of structural damping and acoustic radiation.

3.2 Structural Damping

The primary mechanisms responsible for the damping of metals are associated with dislocations in the crystal lattice and heat conduction between differently strained regions. For aluminum in bending at room temperature a major contribution is made by transverse heat flow from the warmed compression fibers to the cooled tension fibers [16].

The energy dissipated per unit volume of the material can be represented by a hysteresis loop (Figure 3.1). The hatched area represents the energy dissipated. The loop

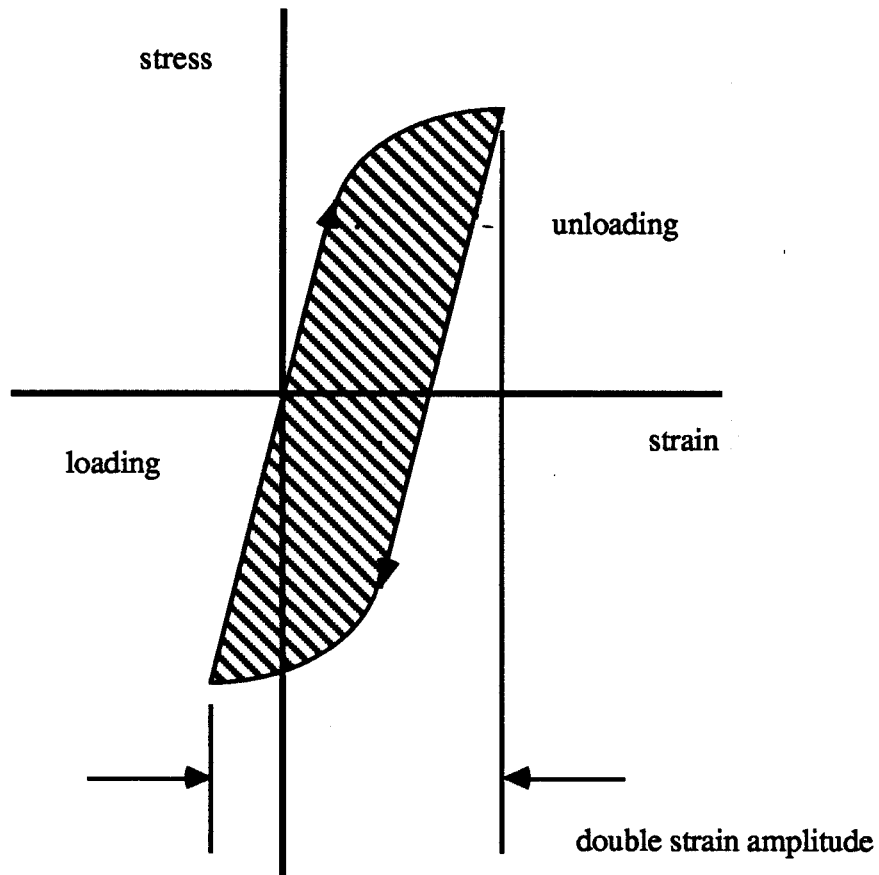


Figure 3.1 ENERGY DISSIPATION

The energy dissipated per unit volume of the material is represented by a hysteresis loop. The hatched area represents the energy dissipated. The loop is formed by stress-strain curves for increasing and decreasing levels of stress and strain. The loop represents one cycle of vibration.

is formed by stress-strain curves for increasing and decreasing levels of stress and strain. The loop thus corresponds to one cycle of vibration. The energy dissipated is approximately proportional to the square of the strain amplitude.

Since the amplitude of vibration is proportional to the strain amplitude, the energy W_d dissipated per cycle can be written as

$$W_d = \gamma X^2 \quad (3.1)$$

where γ is a constant with units of force per displacement, and X is the displacement amplitude. Using the concept of equivalent viscous damping [17], an equivalent viscous damping coefficient C_{eq} can be expressed as

$$\pi C_{eq} \omega X^2 = \gamma X^2$$

or

$$C_{eq} = \gamma / \pi \omega \quad (3.2)$$

where ω is the frequency. Thus, the differential equation of motion for an SDOF system with structural damping may be written as

$$m \frac{d^2 x}{dt^2} + (\gamma / \pi \omega) \frac{dx}{dt} + kx = F(t) \quad (3.3)$$

where m is the mass, x is the displacement, k is the stiffness, and F is the applied force. For simplicity, an SDOF system is considered here. This concept may also be extended to a MDOF system.

If the oscillations are harmonic, equation (3.3) may be written in terms of a complex stiffness

$$m \frac{d^2 x}{dt^2} + (k + j \gamma / \pi) x = F_o \exp j\omega t \quad (3.4)$$

By factoring out the stiffness k and by defining a loss factor $\eta = \gamma / \pi k$, equation (3.4) becomes

$$m \frac{d^2 x}{dt^2} + k(1 + j\eta) x = F_o \exp j\omega t \quad (3.5)$$

Letting $x = X \exp j\omega t$, the steady state solution is obtained as

$$X = \frac{F_o}{(k - m\omega^2) + j\eta k} \quad (3.6)$$

The amplitude at resonance is thus

$$|X| = \frac{F_o}{\eta k} \quad (3.7)$$

Now the resonant response of a system with viscous damping is

$$|X| = \frac{F_o}{2\zeta k} \quad (3.8)$$

where ζ is the viscous damping ratio. Thus at resonance, $\eta = 2\zeta$. The loss factor is thus equal to twice the viscous damping ratio. This relation is important because the direct output of the MDOF complex exponential method is a viscous damping ratio for each mode.

3.3 Radiation Loss

Energy is also lost by radiation from the plate to the surrounding air. Consider a thin plate of infinite size, which has no internal damping, driven to carry a flexural wave of constant amplitude with a phase speed c_p . At a certain arbitrary time, the plate will be deformed as shown in Figure 3.2. A sound wave is radiated outward in the air in such a direction that $\lambda = \lambda_p \sin \theta$. The wavenumber k_p of the flexural wave is

$$k_p = \frac{2\pi f}{c_p} = \frac{2\pi}{\lambda_p} \quad (3.9)$$

Note that the phase speed of a flexural wave is a function of frequency,

$$c_p = \sqrt{\frac{4\omega^2 B}{\rho_s}} \quad (3.10)$$

where B is the bending stiffness of the plate and ρ_s is the mass density of the plate. The sound radiated has a wavenumber

$$k = 2\pi / \lambda = 2\pi / \lambda_p \sin \theta \quad (3.11)$$

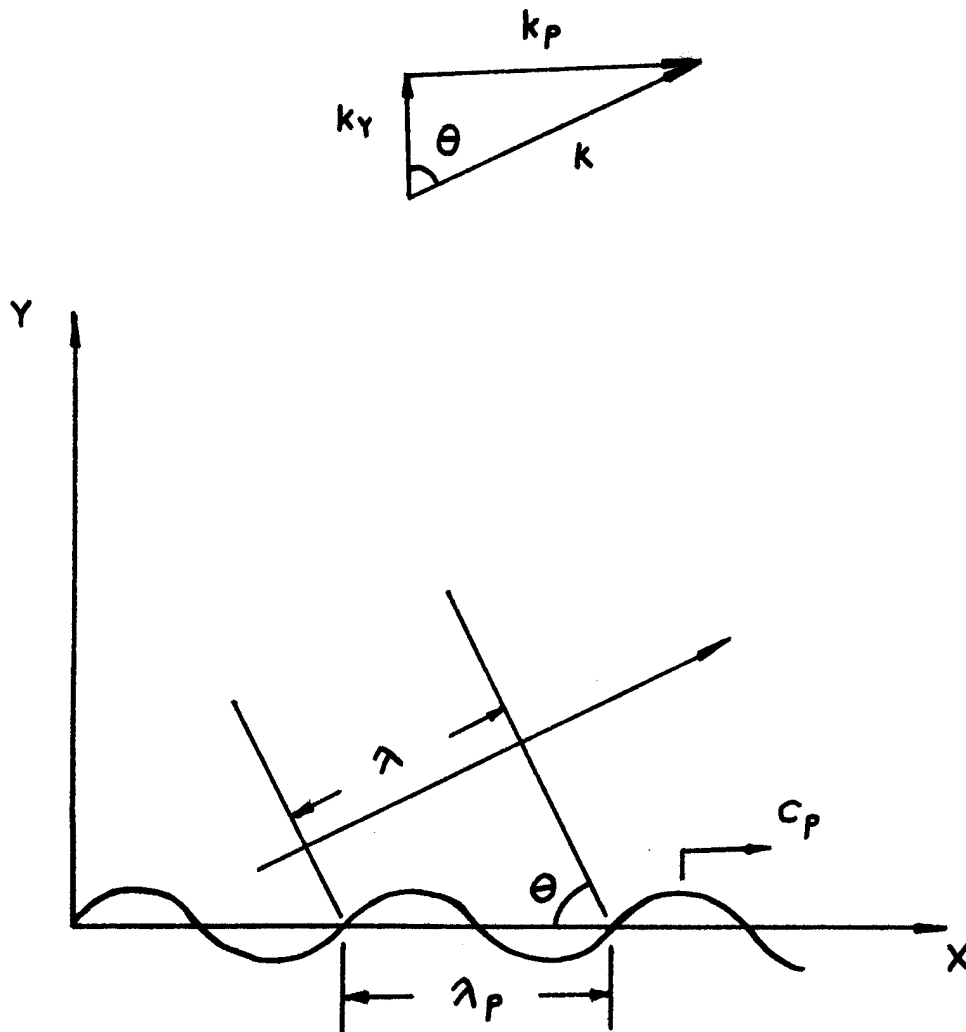


Figure 3.2 ACOUSTIC RADIATION FROM A FLEXURAL WAVE

Consider a thin plate of infinite size, with no internal damping, driven to carry a flexural wave of constant amplitude with a phase speed C_p . At a certain arbitrary time, the plate will be deformed as shown. A sound wave is radiated outward in the air in such a direction that $\lambda = \lambda_p \sin \theta$, where λ is the wavelength of the sound wave and λ_p is the wavelength of the flexural wave. The corresponding wavenumbers form the right triangle relationship shown at the top of the figure, where k_y is the y-component of the sound wavenumber k .

The sound pressure in air above or below the plate is caused by the transverse velocity of the plate vibration. Thus the sound field parallel to the plate has the same spatial periodicity as the plate. The y-component of the acoustic wavenumber forms a vector relationship such that $\mathbf{k} = \mathbf{k}_p + \mathbf{k}_y$. The magnitude and direction of the the acoustical wavenumber k is thus defined by the flexural wavenumber k_p and the frequency.

There are three frequency ranges of interest, which are defined with respect to the critical frequency. The critical frequency is the frequency at which the propagation speed of the flexural wave in the plate equals the speed of sound in the air.

In the region below the critical frequency, $k_p > k$ for an infinte plate with no internal damping. The radiation angle θ is not defined; the sound pressure is 90 degrees out of phase with the plate velocity, and hence no power is radiated. For a finite plate with internal damping, however, a relatively small amount of power will be radiated in this region.

At the critical frequency, $k = k_p$. The radiated sound wave runs parallel to the plate surface with $\theta = 90$ degrees. If the plate velocity could be kept constant, the acoustic pressure and hence the power radiated would approach infinity. In practice, the sound pressure remains finite due to the finite dimensions of the plate and because the loading of the radiating surface is very high under these conditions [14]. Nevertheless, a relatively high amount of power is radiated at this frequency.

In the region above the critical frequency, $k_p < k$. For this case the plate radiates a plane wave into the air at an angle that is determined by the ratio of the wavenumbers

$$\sin \theta = k_p / k = \lambda / \lambda_p \quad (3.12)$$

The sound pressure in the immediate vicinity of the plate is in phase with the plate velocity, and hence power is radiated into the air.

CHAPTER 4

DAMPING MEASUREMENT

4.1 Introduction

In order to use the reverberant field method for power input measurement, the referee structure must be calibrated in terms of a loss factor for each frequency band of interest. There are four common methods for determining loss factors: the reverberant field energy method, the decay method, the half power bandwidth method, the MDOF complex exponential method.

If an electromagnetic shaker is attached to the plate via an impedance head, the power input can be determined from equation (2.12). Using this value along with the mean square velocity in the reverberant field, the loss factor can be obtained from equation (1.2). The reverberant field energy method thus yields the average value of the individual loss factors of the modes in the band. This method is a very convenient method for determining the loss factors. The purpose of this thesis, however, is to verify that the energy method is a valid method for determining power input. Thus, an independent method is needed in order to obtain the loss factors. The decay method and the MDOF complex exponential method are thus considered in this chapter.

4.2 Decay Method

The first independent method considered was the decay method. The decay method is a method by which the loss factor is obtained from the logarithmic decay of the unforced vibration of the structure. A loss factor can be obtained from the reverberation time, which is the time required for the vibrational energy to decay by 60 dB. The relationship between the reverberation time and the loss factor can be derived from the

homogeneous form of the governing differential equation for the energy density in the plate. From equations (2.25) and (2.30),

$$\frac{d\varepsilon}{dt} + \omega\eta\varepsilon = 0 \quad (4.1)$$

Assume a solution of the form

$$\varepsilon = \varepsilon_0 \exp(-t/\tau) \quad (4.2)$$

Taking the derivative of this solution,

$$\frac{d\varepsilon}{dt} = -\varepsilon/\tau \quad (4.3)$$

Substituting equation (4.3) into (4.1) yields

$$\tau = 1/\omega\eta \quad (4.4)$$

Thus equation (4.2) can be rewritten as

$$\varepsilon = \varepsilon_0 \exp(-\omega\eta t) \quad (4.5)$$

The reverberation time T_R is defined as the time required for the energy density to decay by 60 dB. Thus, using equation (4.5),

$$10^{-6} = \exp(-\omega\eta T_R) \quad (4.6)$$

Solving for the loss factor η ,

$$\eta = \frac{-\ln 10^{-6}}{\omega T_R} \quad (4.7)$$

Or

$$\eta \cong \frac{2.2}{f T_R} \quad (4.8)$$

The loss factor can thus be obtained from the reverberation time.

The decay method can be carried out, for example, by striking the plate with a hammer. The resulting acceleration is then measured with an accelerometer. The acceleration signal is then filtered into the desired band. The filtered signal is then recorded on a graphic level recorder. The recorder plots the decay of the logarithm of the envelope of the signal.

In reality, it is impractical to excite the structure and measure the time taken for a full 60 dB decay. Instead, the reverberation time is estimated from the slope of the decay plot. If all of the modes in a particular frequency band have the same amount of damping and if the damping is linear, the decay plot will be a straight line. In this case the frequency band loss factor can be accurately estimated.

Generally, the modes in a frequency band will have differing amounts of damping. In the decay plot, the effect of the higher damped modes is quickly lost while the effect of the lower damped modes lingers on. The decay plot may thus be curved as shown in Figure 4.1. A single unambiguous slope value cannot be selected in this case. The initial slope of the decay should represent the best average damping. But this slope is generally too short to measure with precision.

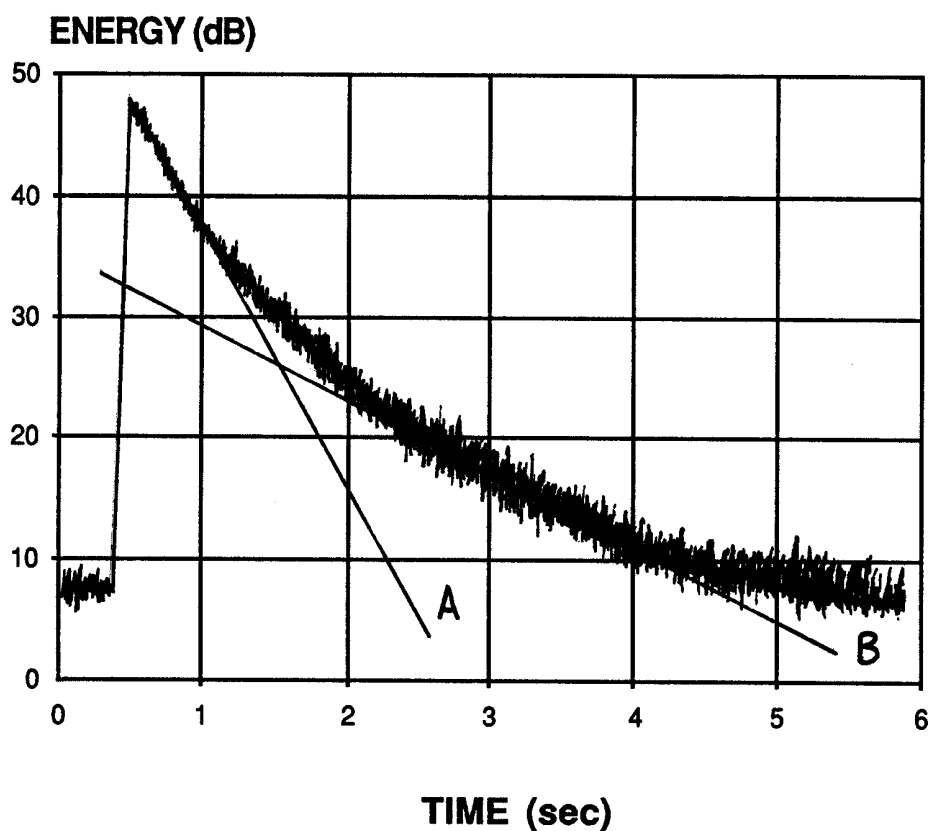


Figure 4.1 TYPICAL DECAY CURVE

The energy decay in the 500 - 1000 Hz frequency band for 1/4 in thick plate is shown. The plate was excited by a hammer strike. If all the modes in this band had similar loss factors, then the logarithmic energy decay would be linear. The modes, however, decay at different rates. The slope of the decay thus varies with time. Slope "A" represents a loss factor of 0.0011. Slope "B" represents a loss factor of 0.0003. The MDOF complex exponential method and the reverberant field energy method each yielded a value of 0.0011 for this case.

In addition, there are several other problems which can occur in making reverberation time measurements. There may be acoustic coupling between the room and the plate. As the plate radiates sound energy into the room, the room may return some of the energy to the plate at a later time. Furthermore, the writing speed of the graphic level recorder may be slower than the energy decay. For these reasons, the decay method appears to be an unreliable method for calibrating plates.

4.3 MDOF complex exponential method

The decay method operates on the transient response of the plate. Many of the problems encountered with making decay measurements are eliminated by using a steady state approach. There are a number of methods which estimate loss factors based upon the frequency response functions. The half power bandwidth method is perhaps the most familiar of these methods. The half power bandwidth method, however, is an SDOF method which assumes that the total response is dominated by a single mode in the vicinity of resonance.

For structures with closely-spaced modes, the half power bandwidth method is inappropriate. The plates used in this thesis have a relatively high modal density and hence display severe modal overlapping in the frequency response functions, particularly above the critical frequency. Thus, the MDOF complex exponential method was chosen to measure the loss factors. This method is a multi-mode curve-fitting technique which is well suited for structures with closely-spaced modes.

A mathematical description of the MDOF complex exponential method is given in appendix D. A brief overview of the method is given here. The method is carried out by obtaining a frequency response function over a frequency range of interest either by means of an impedance head or by means of a force transducer and an accelerometer where the accelerometer is mounted at a point away from the force input. The modal

parameters are then solved for by using a series of impulse response functions which are obtained through an inverse Fourier transform of the frequency response function. Based upon the calculated modal parameters, a regenerated frequency response function is then constructed and superimposed upon the original frequency response function. A number of roots are also output in numerical form. These roots are in the form of frequencies and corresponding damping ratios. The number of roots will exceed the number of modes in the frequency response function. The excess roots represent 'computational' modes which serve to account for the slight imperfection inevitably present in measured data. These computational modes often have damping ratios which are ridiculously high or low. Thus, the user must use judgement in selecting the roots which actually represent the modes. This is done by graphically observing the agreement between the original and regenerated frequency response functions and by numerically checking the agreement between the frequencies of the roots and the frequencies of the peaks in the original frequency response function.

The number of roots solved for can be varied by the user in order to obtain the optimum agreement between the original and the regenerated frequency response function. The MDOF complex exponential method is thus a trial and error procedure.

CHAPTER 5

EXPERIMENTAL RESULTS

A 1/4 inch thick and a 1/2 in thick aluminum plate were used as referee structures. Each plate had surface dimensions of 4 ft by 6.5 ft. The plates were suspended vertically by elastic cords which were attached to a frame as shown in Figure 5.1. This was done to approximate free boundary conditions and to minimize energy losses at the boundaries. Furthermore, no external damping material was applied to the plates. A diagram of the complete equipment set-up is given in Figure 5.2. An accompanying listing of the instrumentation is given in Table 5.1.

The plates were calibrated by measuring the frequency response functions obtained from the force input by the shaker and from the acceleration measured by accelerometers at various locations on the plates. The loss factors of individual modes were then obtained by using the MDOF complex exponential method. The band average loss factors were then obtained from the arithmetic average of the loss factors of the individual modes. The loss factors obtained for the 1/4 in and the 1/2 in thick plates are shown in Figures 5.3 and 5.4, respectively.

Next, the vibrational input power measurements were made. The potential across the shaker was set at six different levels: 2.0 V, 2.5 V, 3.0 V, 3.5 V, 4.0 V, and 4.5 V. This was done in order to test the linearity of the system. The vibrational power input from the shaker into the plate was then obtained for each of these cases for both plates from the force and acceleration signals from the impedance head. The power was calculated according to equation (2.12). The acceleration in the reverberant field was measured by an accelerometer. The corresponding velocity was calculated according to equation (1.7). The accelerometer was positioned at ten different locations in order to obtain a spatial average.

The power input for each case was then calculated from the reverberant field velocity by equation (1.2). The results were average over 500 Hz constant bandwidths for the frequency range 0-4000 Hz. A comparison was then made between the reverberant field method results and the impedance head results for each of the cases. The power input comparisons for the six input voltage cases are shown in Figures 5.5 through 5.10 for the 1/4 in thick plate and in Figures 5.11 through 5.16 for the 1/2 in thick plate. The average error between the two methods is given in Figure 5.17 for the 1/4 in plate and in Figure 5.18 for the 1/2 in plate.

In addition, the impedance head power measurements and the velocity measurements were used to calculate loss factors by equation (1.2). These loss factors were compared with the loss factors obtained from the MDOF complex exponential method. The comparisons for the 1/4 in and the 1/2 in thick plates are given in Figures 5.19 and 5.20, respectively.

Based upon the loss factors and the experimental conditions, the difference between the direct field and the reverberant field energy densities was calculated according to equations (1.2) and (1.3). This was done in order to verify that the direct field strength was sufficiently below the reverberant field strength. The calculated differences for the 1/4 in and 1/2 in plates are given in Figures 5.21 and 5.22, respectively.

Measurements of the point impedance were also made. Spatial averages of the results for the 1/4 in and the 1/2 in plates are given in Figures 5.23 and 5.24, respectively. Finally, one side of the 1/4 in plate was completely covered with a layer of viscoelastic damping material in order to determine how this change in damping would effect the point impedance. The results are shown in Figure 5.25. Determining the optimum amount of damping for a referee plate is an area where additional research is needed.

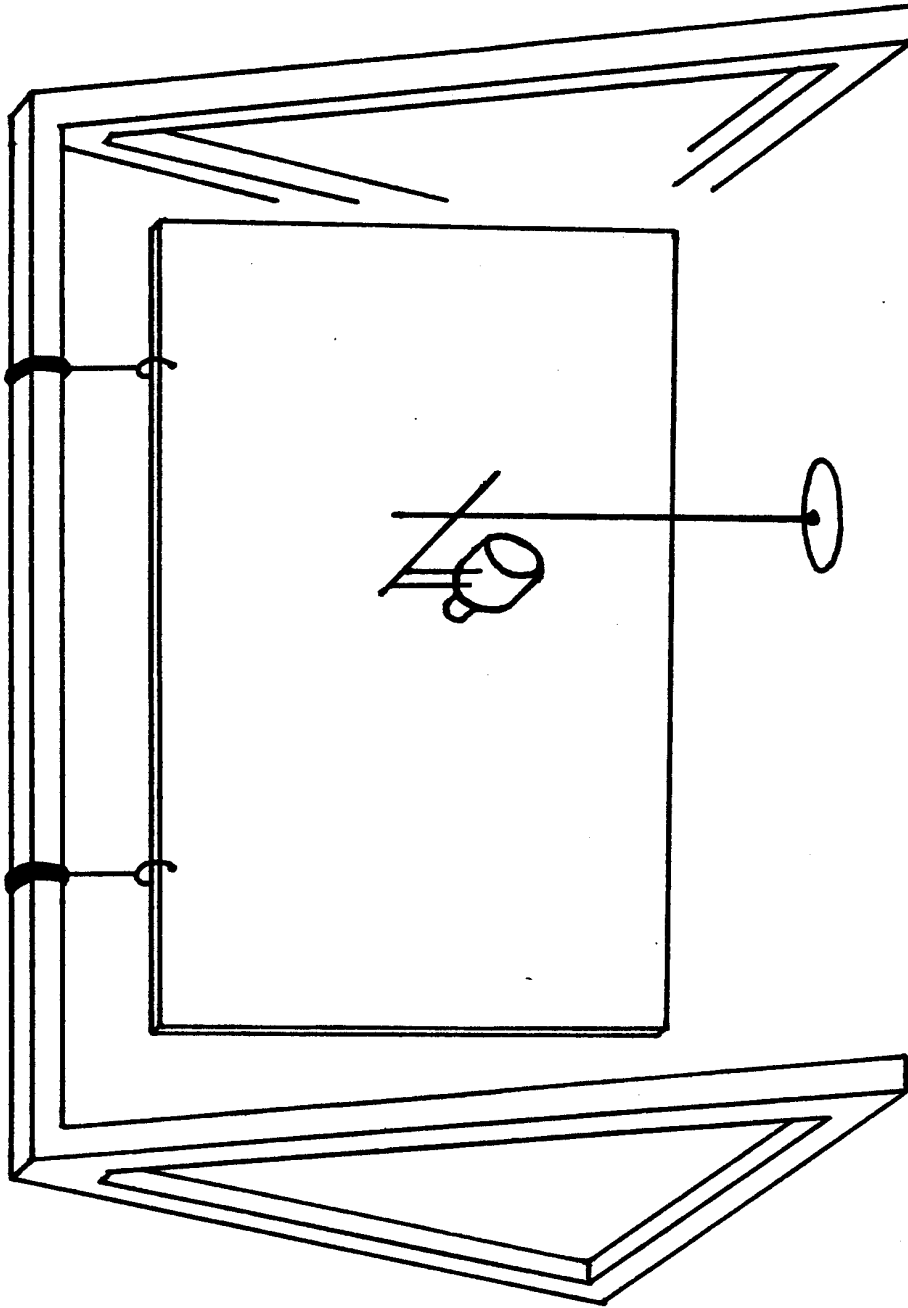


Figure 5.1 PLATE AND SHAKER

A 4.0 by 6.5 foot plate is suspended vertically by elastic cords which are attached to the frame. The shaker is the large cylinder near the center of the plate. The shaker is attached to the plate via an impedance head, the smaller cylinder.

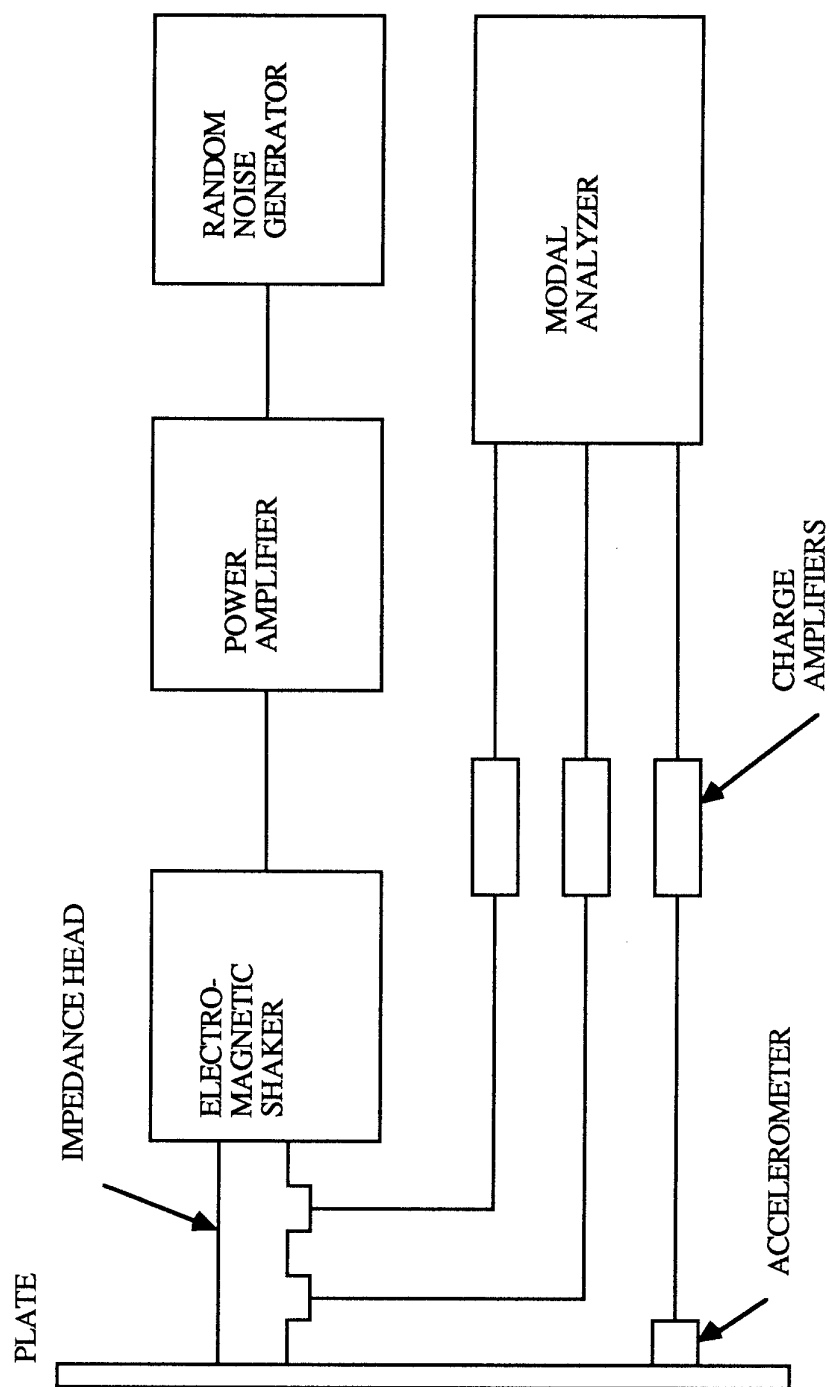


Figure 5.2 EQUIPMENT SET-UP

An amplified random noise signal is input into the shaker. The shaker then transmits vibrational power into the plate via an impedance head. The impedance head has one transducer which measures the force input and another which measures the acceleration at the input point. The acceleration at other points is measured by an accelerometer. The analog signals from these transducers are fed into the modal analyzer where they are converted into digital signals. The model name of each component is given in table 5.1.

Table 5.1 INSTRUMENTATION LIST

Random Noise Generator:	GenRad 1390-B
Power Amplifier:	Krohn-Hite UF-101
Shaker:	Bruel and Kjaer 4810
Impedance Head:	PCB Piezotronics 288M04
Plate:	Reynolds Aluminum
Accelerometer:	PCB Piezotronics 303A03
Charge Amplifiers:	PCB Piezotronics 480A
Modal Analyzer:	GenRad 2510

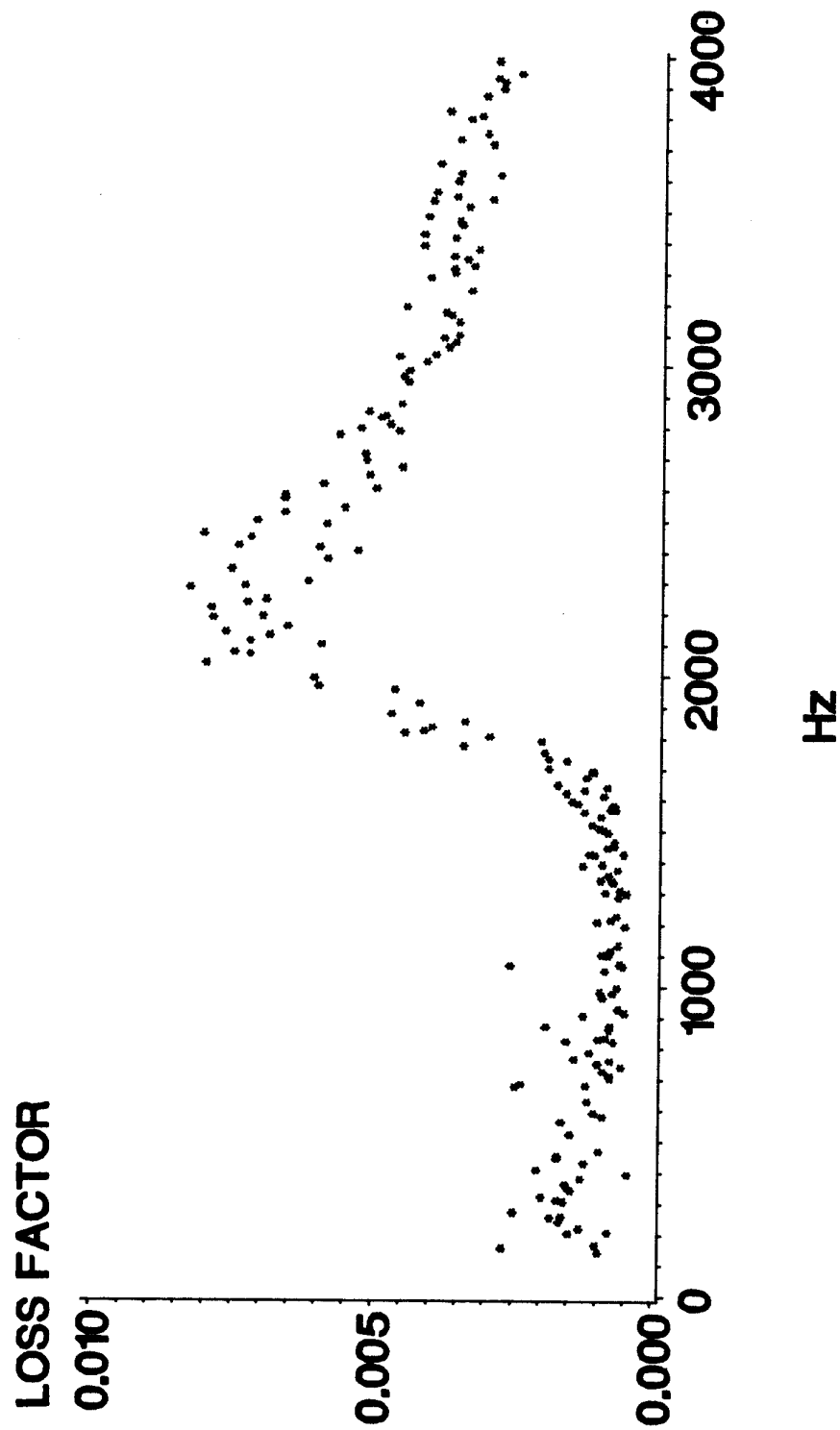


Figure 5.3 INDIVIDUAL LOSS FACTORS FOR THE 1/4 IN THICK PLATE

The loss factors were obtained for individual modes by the MDOF complex exponential method. The theoretical critical frequency is 2000 Hz. At this frequency the phase speed of the flexural waves in the plate is equal to the speed of sound in the air. Above this frequency the losses are dominated by acoustic radiation.

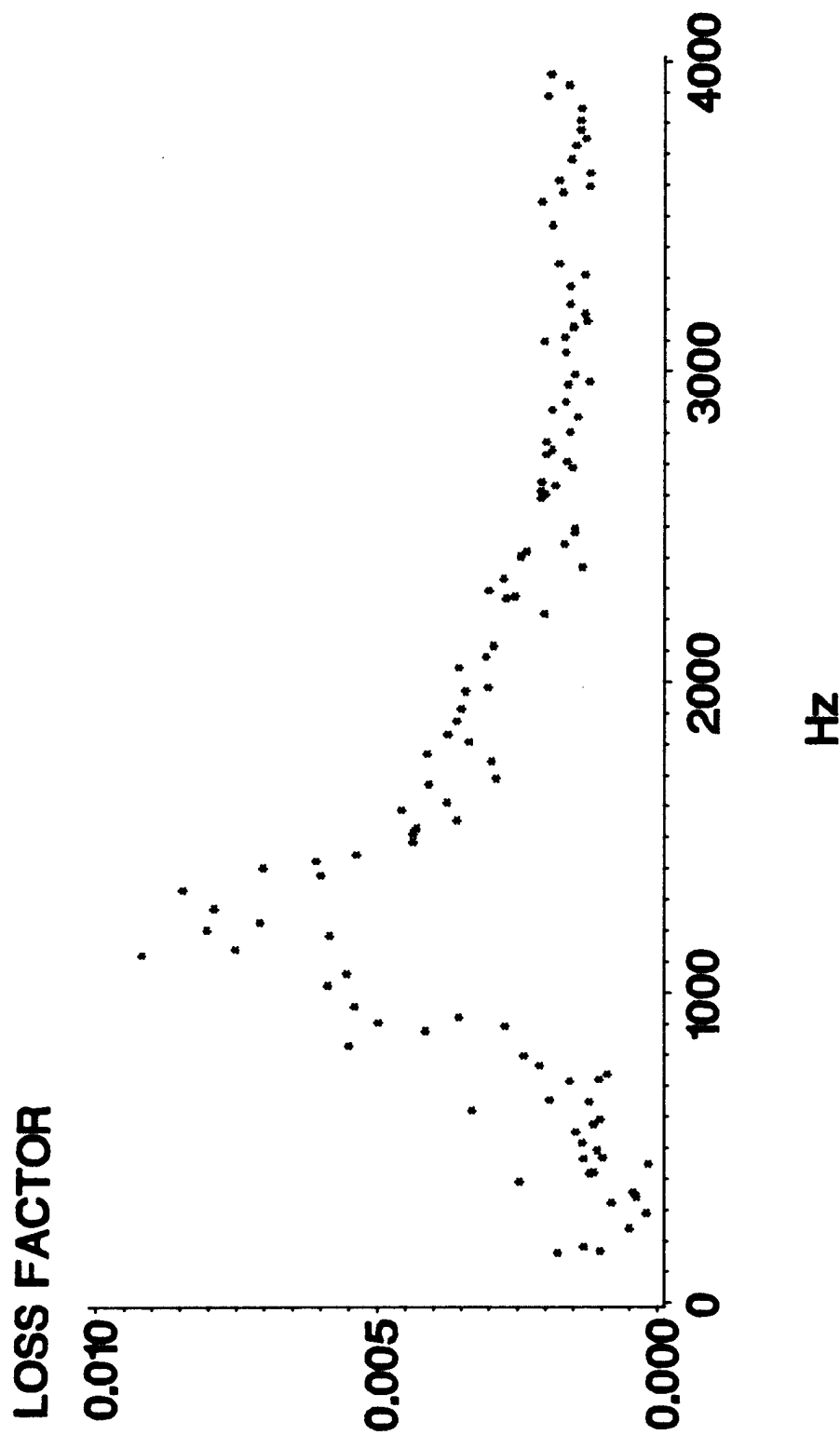


Figure 5.4 INDIVIDUAL LOSS FACTORS FOR THE 1/2 IN THICK PLATE

The loss factors were obtained for individual modes by the MDOF complex exponential method. The theoretical critical frequency is 1000 Hz. At this frequency the phase speed of the flexural waves in the plate is equal to the speed of sound in the air. Above this frequency the losses are dominated by acoustic radiation.

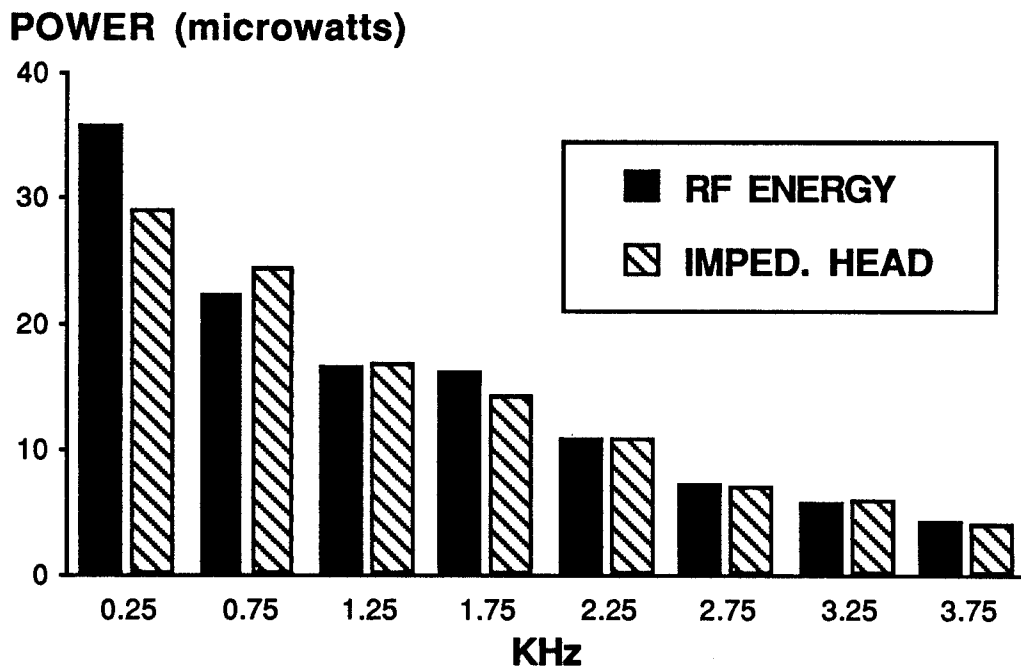


Figure 5.5 POWER INPUT INTO 1/4 IN THICK PLATE, 2.0 V CASE

The vibrational power was measured by the reverberant field energy method (RF ENERGY) and by the force and acceleration signals from the impedance head (IMPED. HEAD). The results are given in 500 Hz constant bandwidths. The vibrational power was input by an electromagnetic shaker attached to the plate via an impedance head. The potential across the shaker was set at 2.0 V for this case.

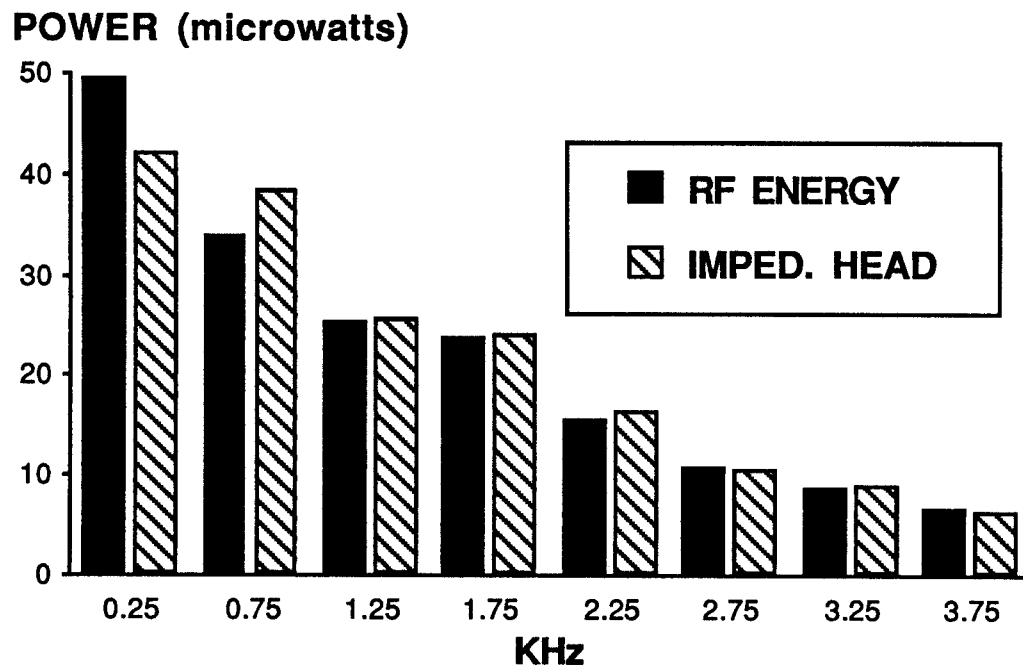


Figure 5.6 POWER INPUT INTO 1/4 IN THICK PLATE, 2.5 V CASE

This is the same as figure 5.5 with the potential across the shaker set at 2.5 V.

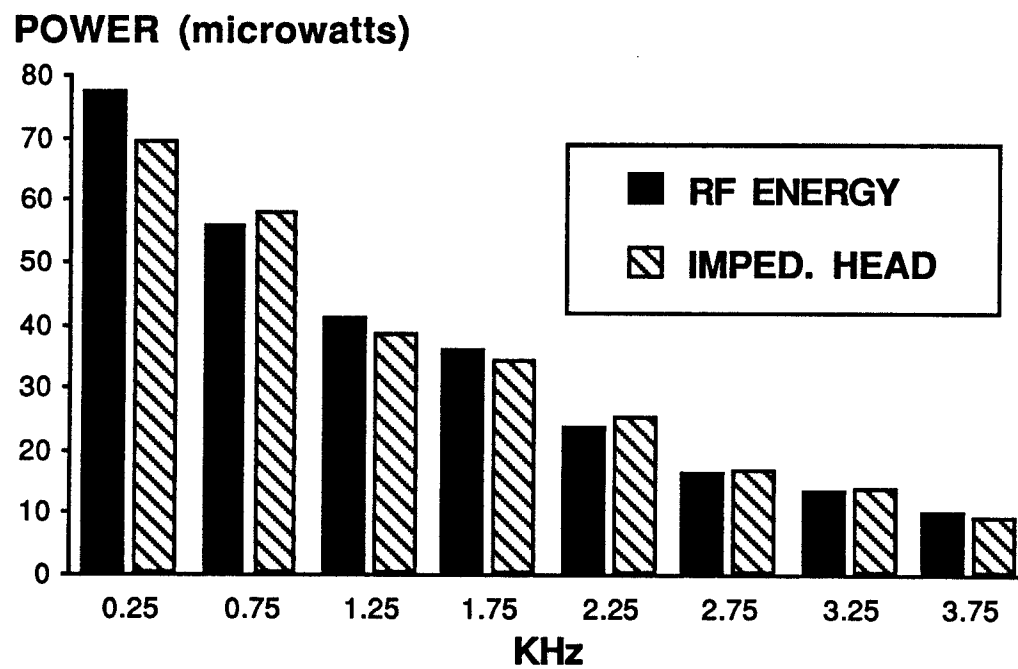


Figure 5.7 POWER INPUT INTO 1/4 IN THICK PLATE, 3.0 V CASE

This is the same as figure 5.5 with the potential across the shaker set at 3.0 V.

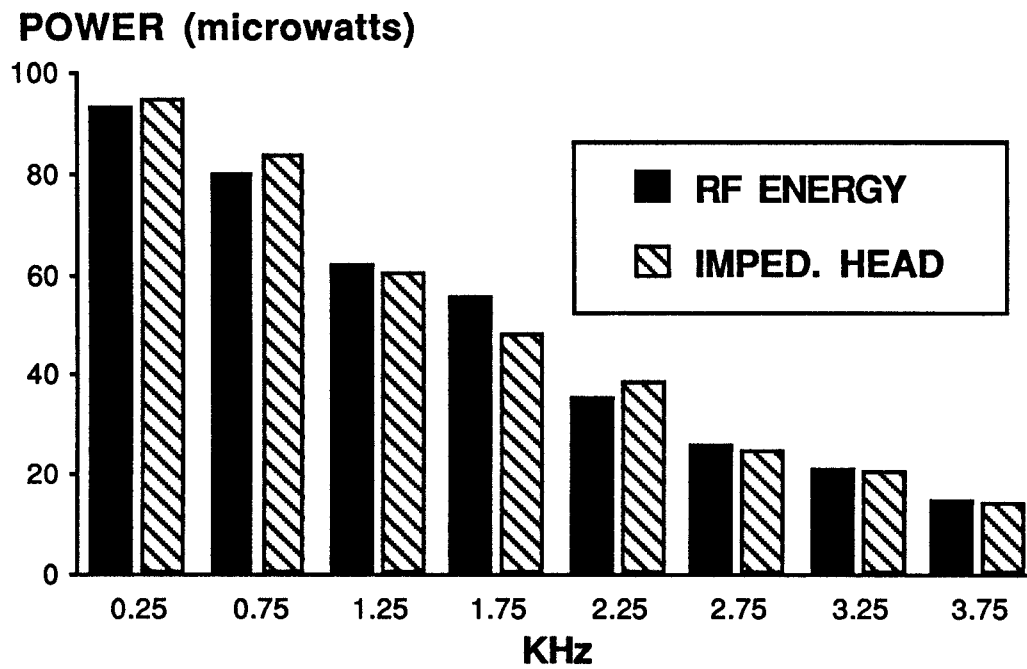


Figure 5.8 POWER INPUT INTO 1/4 IN THICK PLATE, 3.5 V CASE

This is the same as figure 5.5 with the potential across the shaker set at 3.5 V.

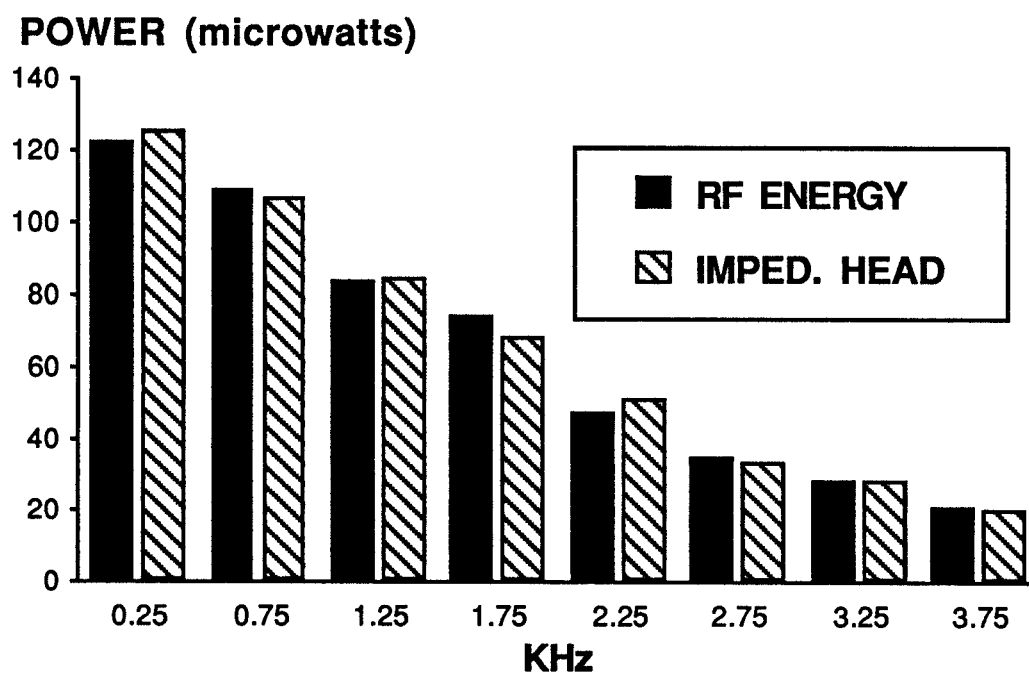


Figure 5.9 POWER INPUT INTO 1/4 IN THICK PLATE, 4.0 V CASE

This is the same as figure 5.5 with the potential across the shaker set at 4.0 V.

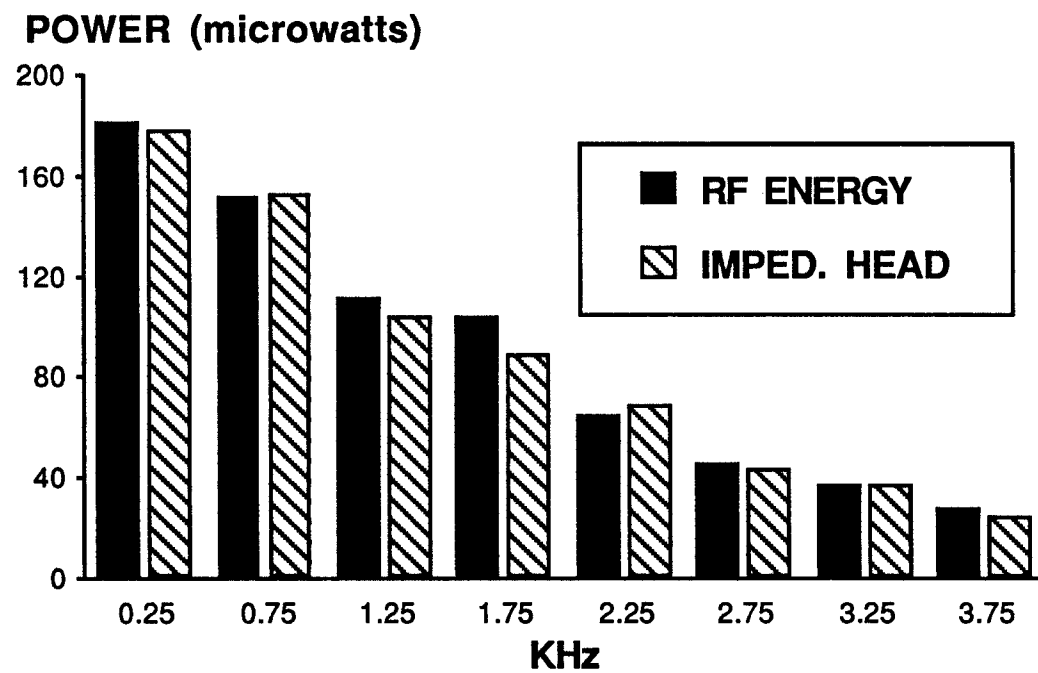


Figure 5.10 POWER INPUT INTO 1/4 IN THICK PLATE, 4.5 V CASE

This is the same as figure 5.5 with the potential across the shaker set at 4.5 V.

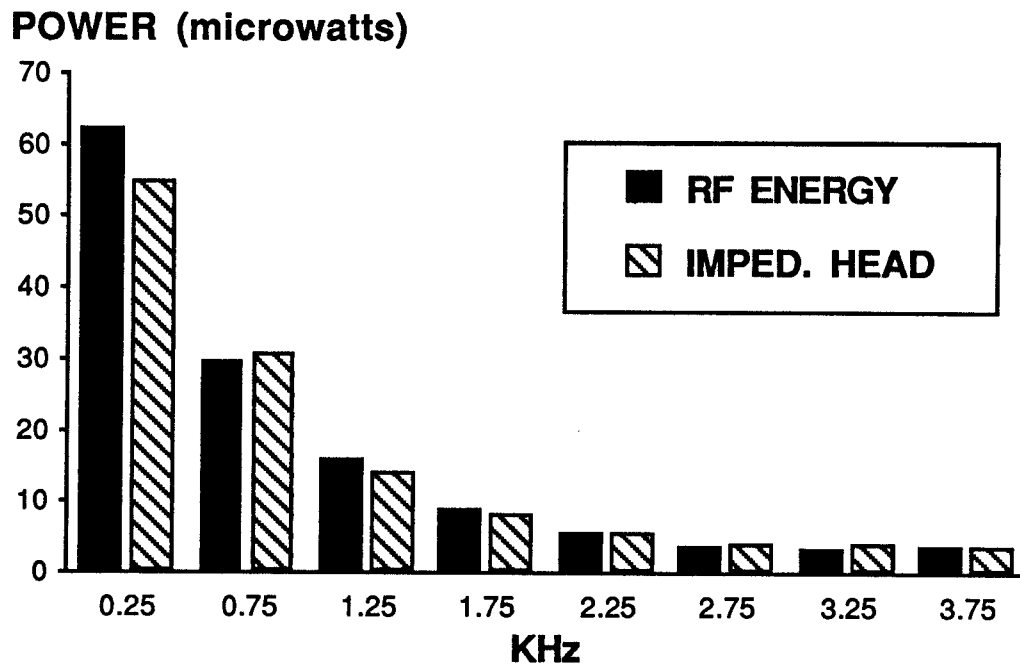


Figure 5.11 POWER INPUT INTO 1/2 IN THICK PLATE, 2.0 V CASE

The vibrational power was measured by the reverberant field energy method (RF ENERGY) and by the force and acceleration signals from the impedance head (IMPED. HEAD). The results are given in 500 Hz constant bandwidths. The vibrational power was input by an electromagnetic shaker attached to the plate via an impedance head. The potential across the shaker was set at 2.0 V for this case.

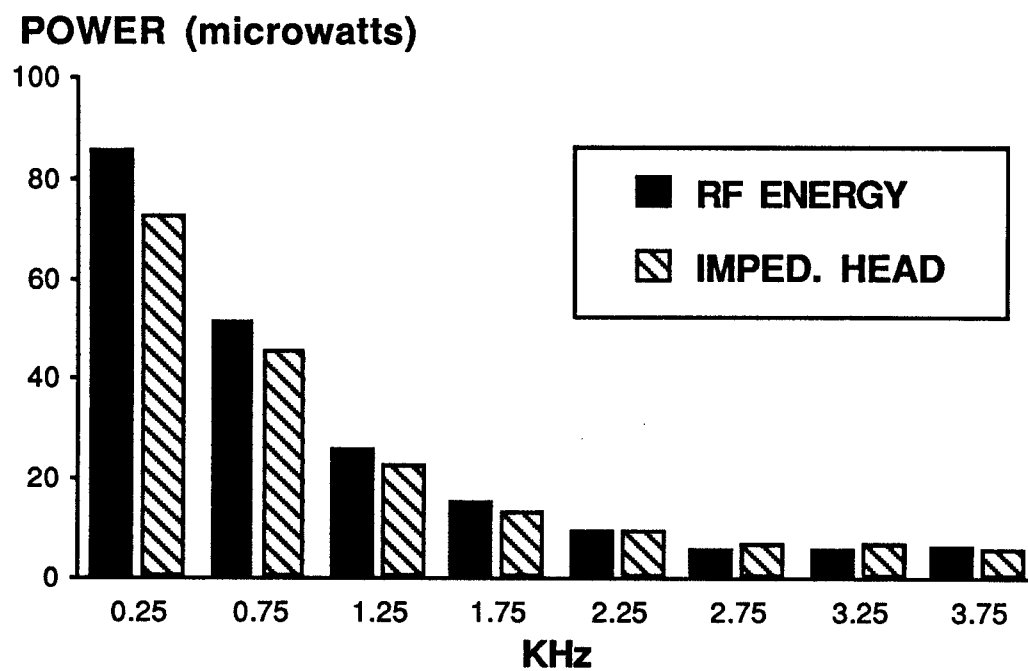


Figure 5.12 POWER INPUT INTO 1/2 IN THICK PLATE, 2.5 V CASE

This is the same as figure 5.11 with the potential across the shaker set at 2.5 V.

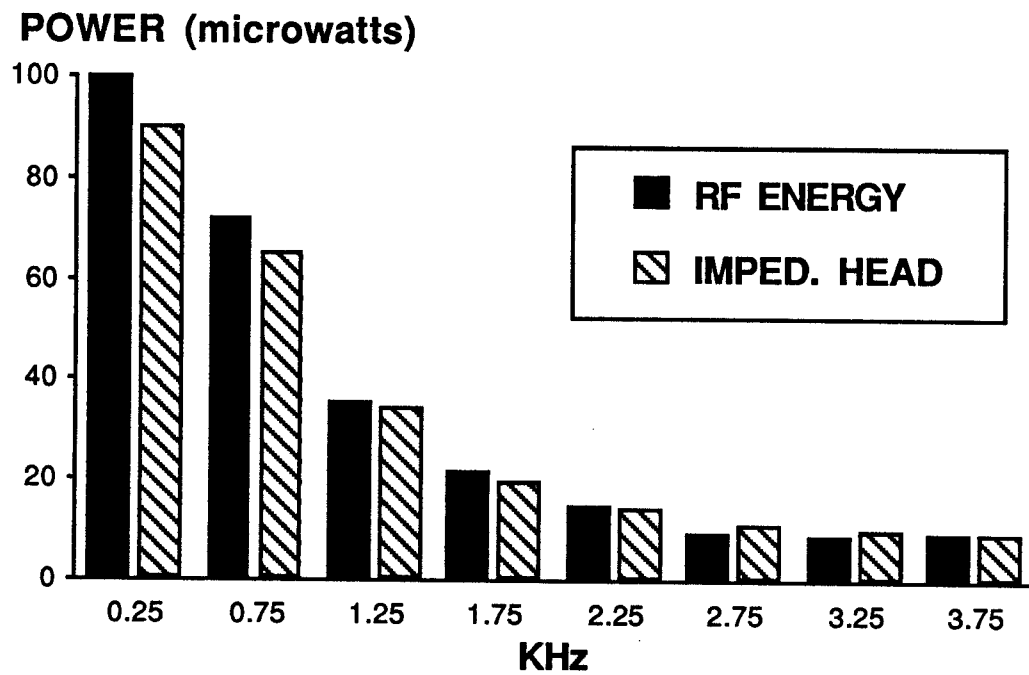


Figure 5.13 POWER INPUT INTO 1/2 IN THICK PLATE, 3.0 V CASE

This is the same as figure 5.11 with the potential across the shaker set at 3.0 V.

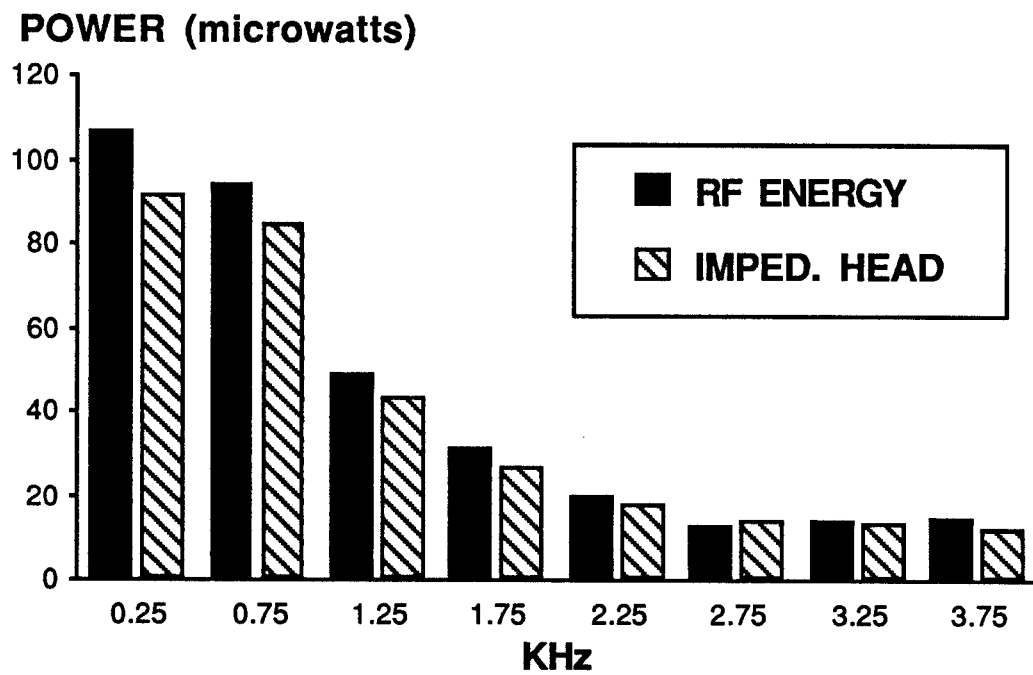


Figure 5.14 POWER INPUT INTO 1/2 IN THICK PLATE, 3.5 V CASE

This is the same as figure 5.11 with the potential across the shaker set at 3.5 V.

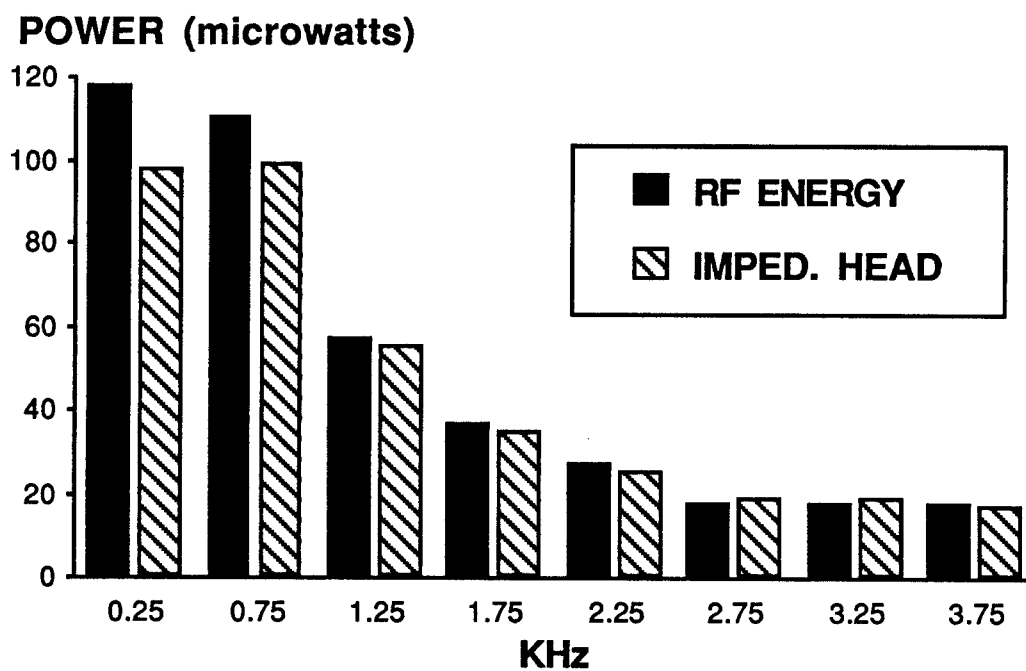


Figure 5.15 POWER INPUT INTO 1/2 IN THICK PLATE, 4.0 V CASE

This is the same as figure 5.11 with the potential across the shaker set at 4.0 V.

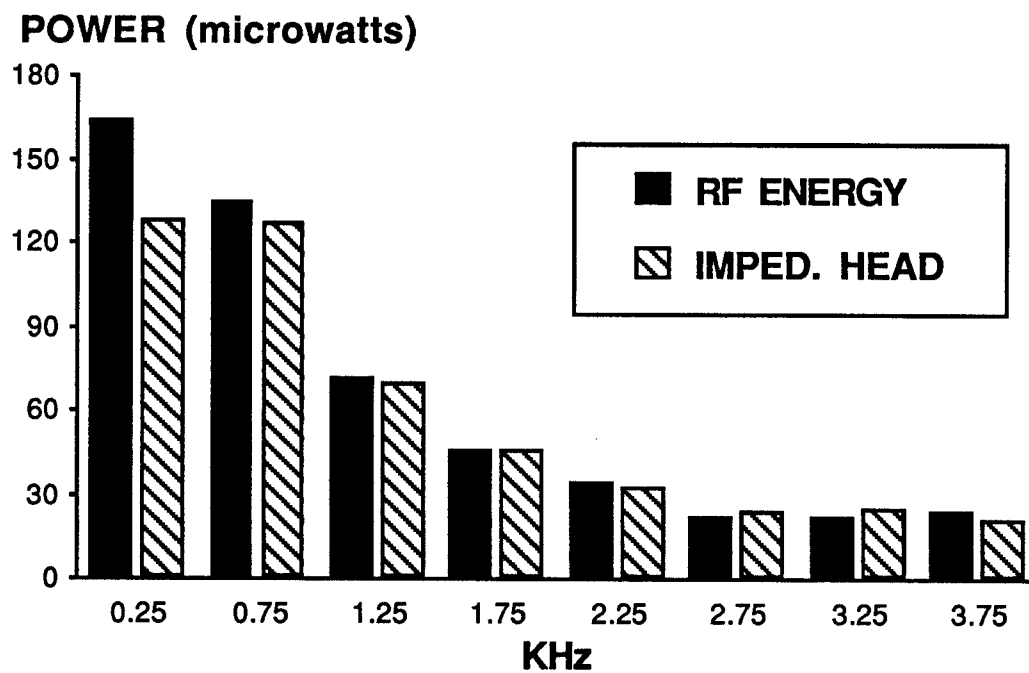


Figure 5.16 POWER INPUT INTO 1/2 IN THICK PLATE, 4.5 V CASE

This is the same as figure 5.11 with the potential across the shaker set at 4.5 V.

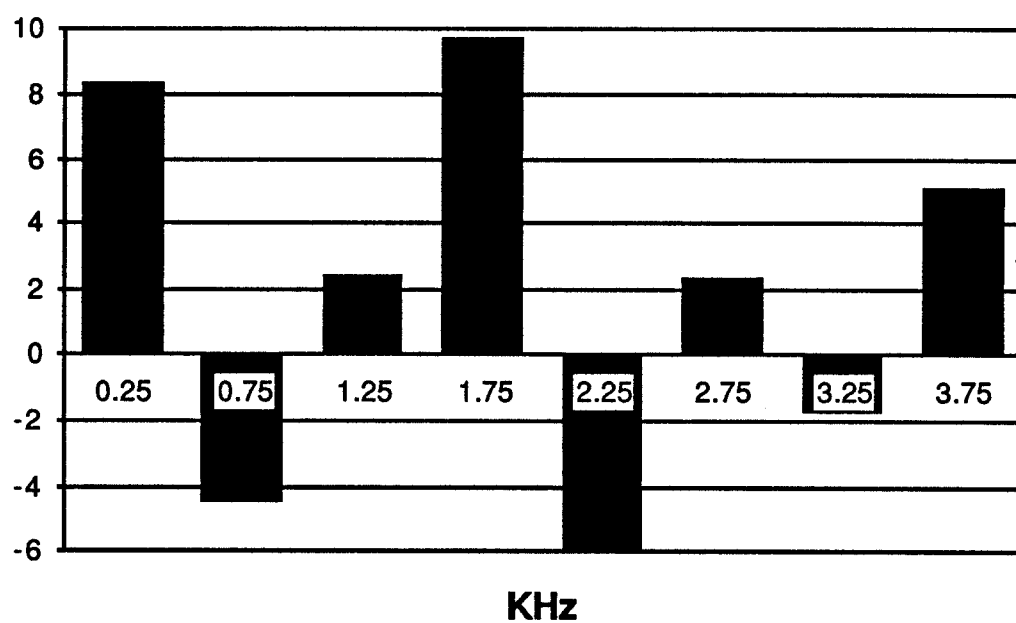
% ERROR

Figure 5.17 AVERAGE ERROR FOR 1/4 IN THICK PLATE

The error in power measured by the reverberant field method with respect to the impedance head method is shown here. The error is averaged from the six shaker voltage cases.

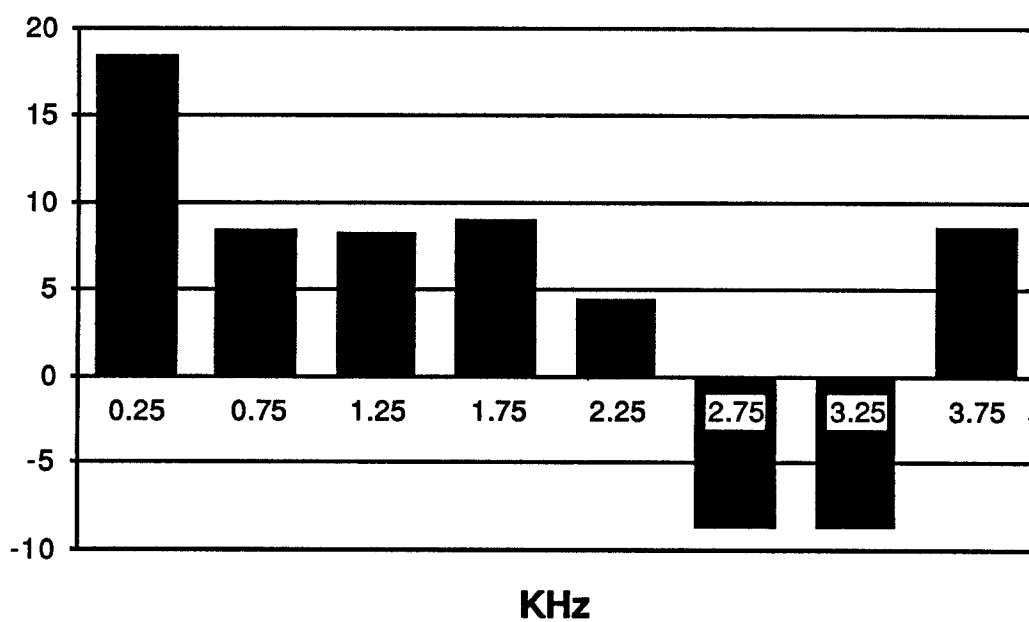
% ERROR

Figure 5.18 AVERAGE ERROR FOR 1/2 IN THICK PLATE

The error in power measured by the reverberant field method with respect to the impedance head method is shown here. The error is averaged from the six shaker voltage cases.

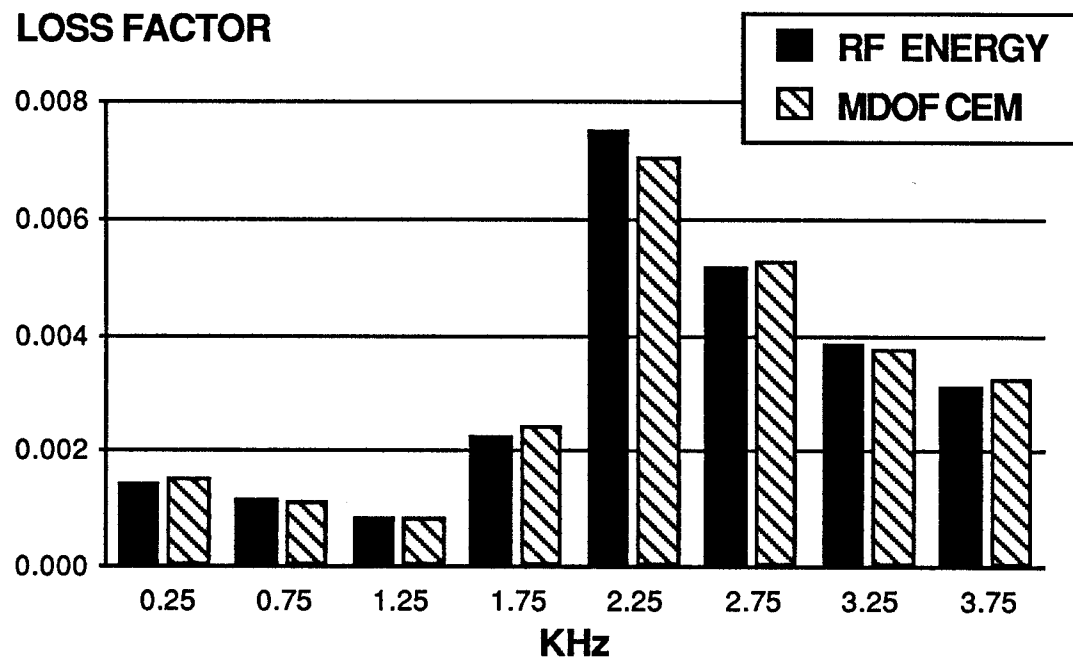


Figure 5.19 AVERAGE LOSS FACTORS FOR 1/4 IN THICK PLATE

The average loss factors obtained for 500 Hz constant bandwidths for the 1/4 in thick plate are shown. The loss factors were obtained by the reverberant field energy method (RF ENERGY) and by the multi-degree-of-freedom complex exponential method (MDOF CEM). The theoretical critical frequency is 2000 Hz. Above this frequency the losses are dominated by acoustic radiation.

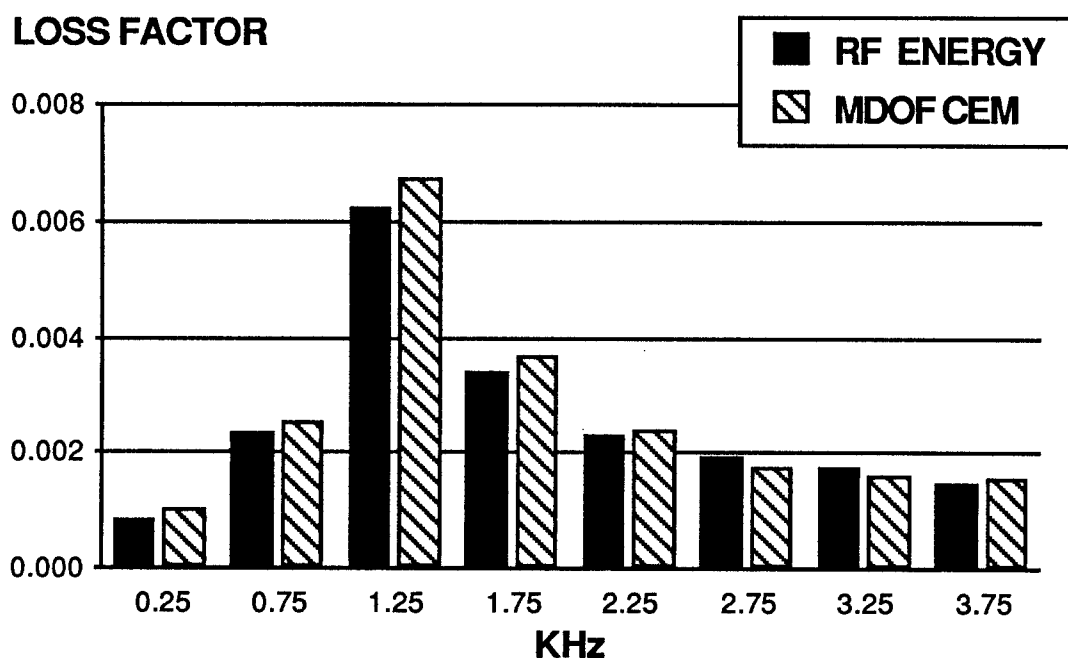


Figure 5.20 AVERAGE LOSS FACTORS FOR 1/2 IN THICK PLATE

The average loss factors obtained for 500 Hz constant bandwidths for the 1/2 in thick plate are shown. The loss factors were obtained by the reverberant field energy method (RF ENERGY) and by the multi-degree-of-freedom complex exponential method (MDOF CEM). The theoretical critical frequency is 1000 Hz. Above this frequency the losses are dominated by acoustic radiation.

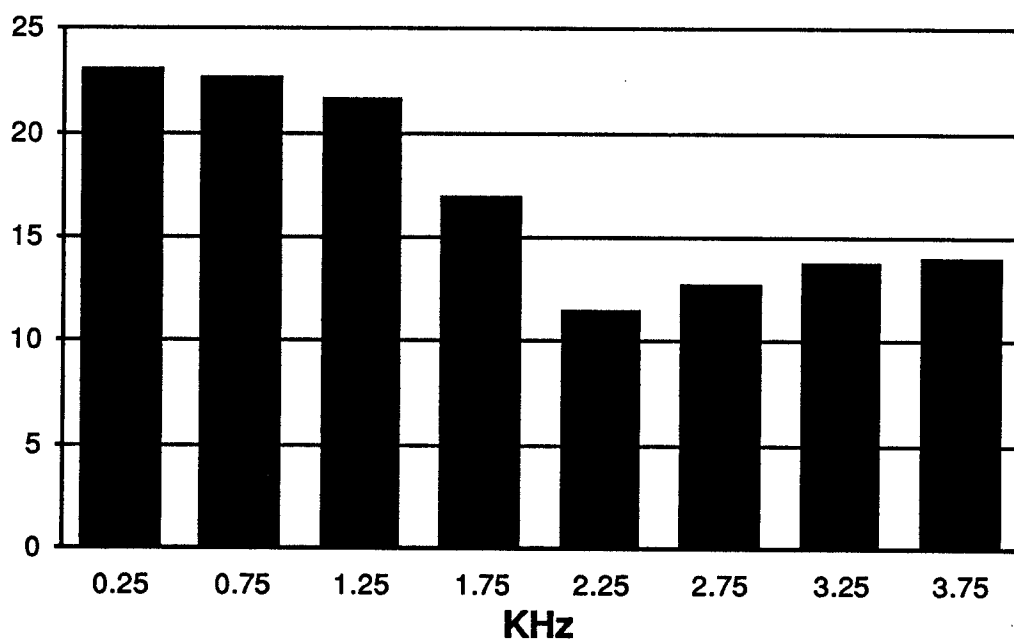
DIFFERENCE (dB)

Figure 5.21 DIFFERENCE IN ENERGY DENSITIES FOR 1/4 THICK PLATE

This graph shows difference between the reverberant field energy density and the direct field energy density, where the difference = $10 \log[\epsilon_r / \epsilon_d]$. The energy densities were calculated from equations (1.3) and (1.4) using the measured loss factors. The losses were assume to be entirely due to surface loss for the purpose of these calculations.

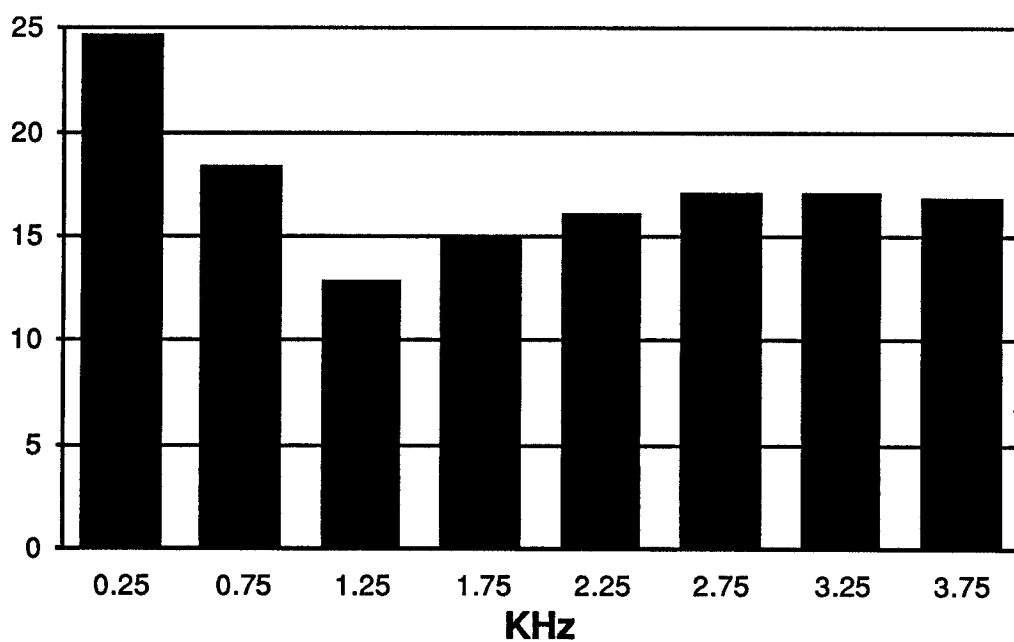
DIFFERENCE (dB)

Figure 5.22 DIFFERENCE IN ENERGY DENSITIES FOR 1/2 THICK PLATE

This graph shows difference between the reverberant field energy density and the direct field energy density, where the difference = $10 \log[\epsilon_r / \epsilon_d]$. The energy densities were calculated from equations (1.3) and (1.4) using the measured loss factors. The losses were assume to be entirely due to surface loss for the purpose of these calculations.

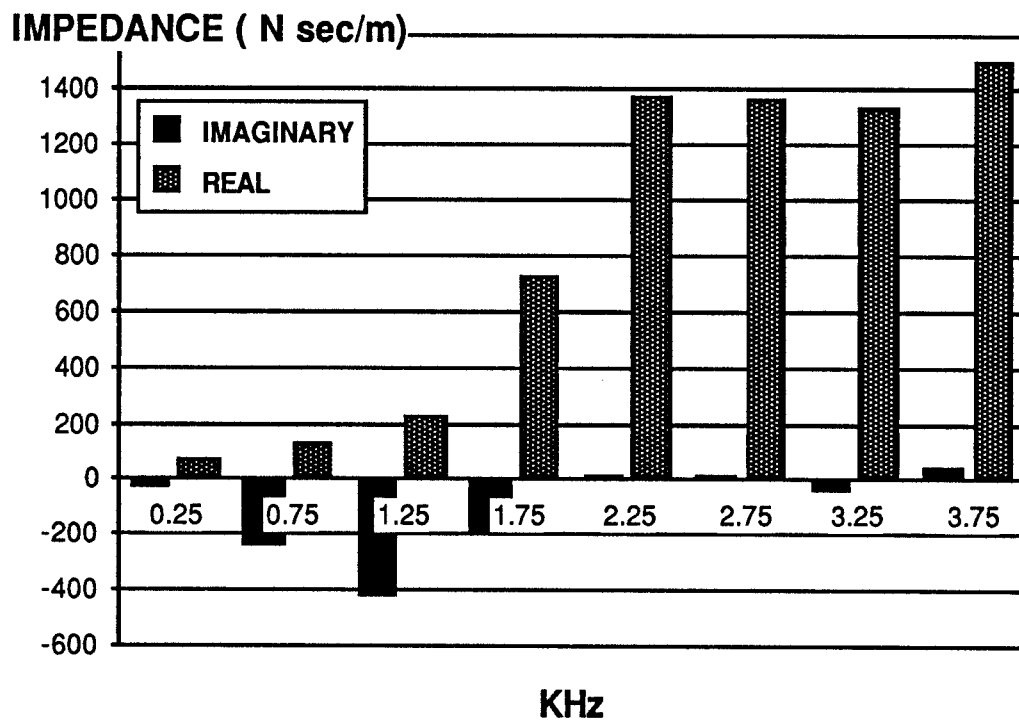


Figure 5.23 MECHANICAL POINT IMPEDANCE OF 1/4 IN THICK PLATE

The spatial averaged point impedance is shown in terms of its real and imaginary components. The theoretical real value for an infinite 1/4 in thick aluminum plate is 1373 N sec/m. The theoretical imaginary value for an infinite plate is zero.

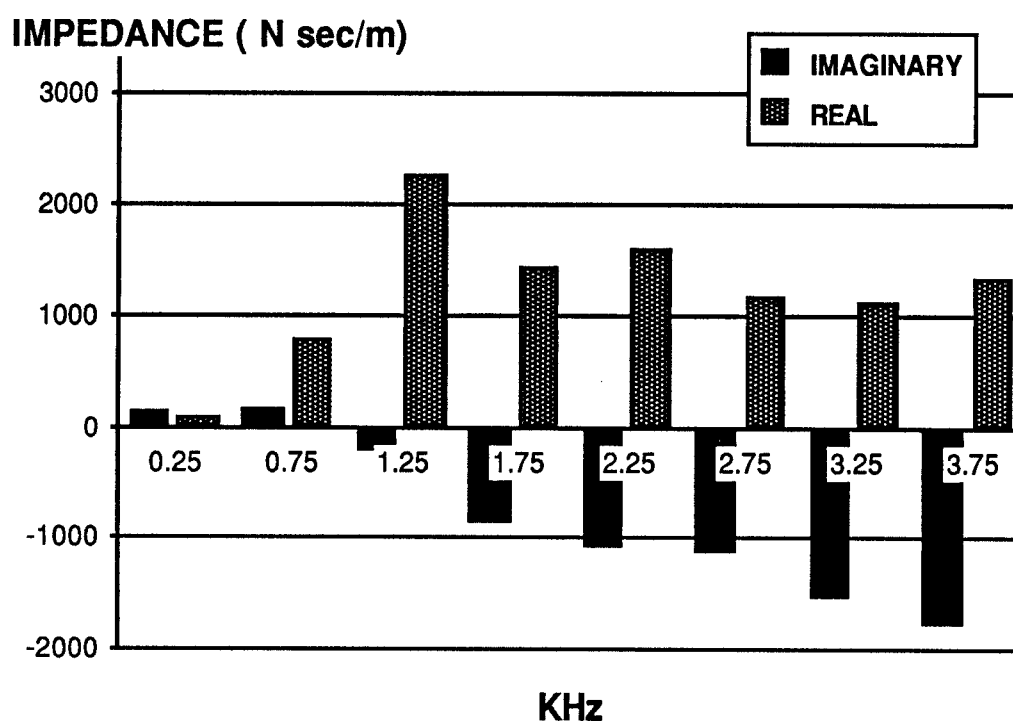


Figure 5.24 MECHANICAL POINT IMPEDANCE OF 1/2 IN THICK PLATE

The spatial averaged point impedance is shown in terms of its real and imaginary components. The theoretical real value for an infinite 1/2 in thick aluminum plate is 5492 N sec/m. The theoretical imaginary value for an infinite plate is zero. For a finite plate with no damping, however, the point impedance is purely imaginary. Thus, the imaginary components obtained for this case are due to the finite dimensions and the relatively low damping of the plate.

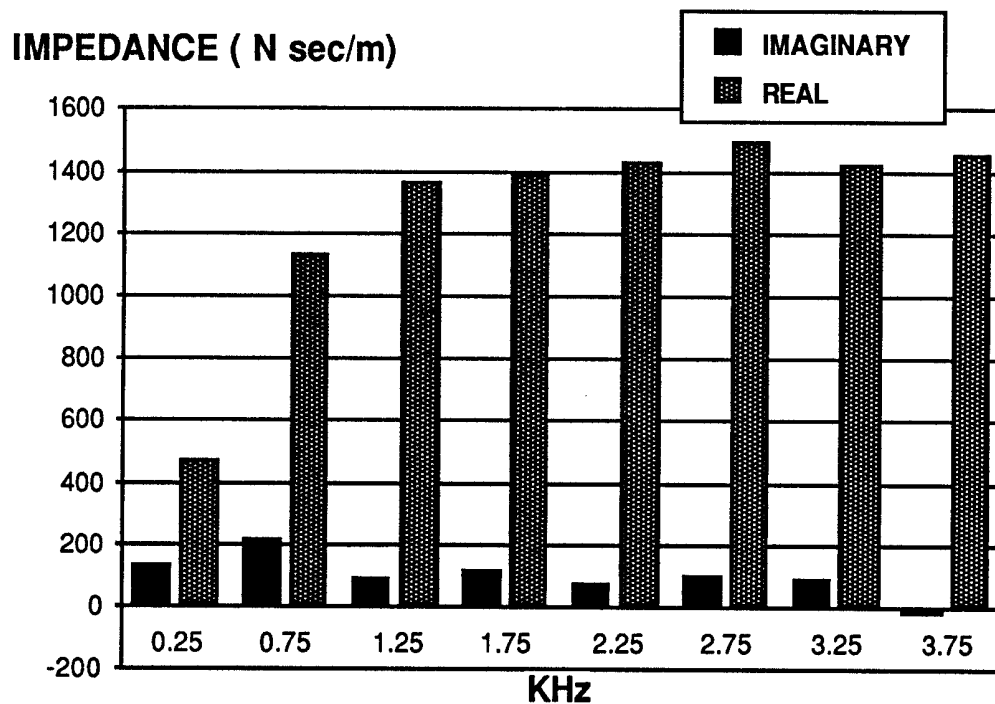


Figure 5.25 MECHANICAL POINT IMPEDANCE OF 1/4 IN THICK PLATE WITH AN EXTERNAL DAMPING TREATMENT

For this case one side of the 1/4 in thick plate was completely covered with a thin layer of viscoelastic damping material. The mass of the damping material is negligible with respect to the mass of the plate. Thus, the theoretical real impedance is still 1373 N sec/m. The damping material had the effect of raising the experimental impedance below the critical frequency, 2000 Hz. Above the critical frequency, the impedance values remained approximately the same as those shown in figure 5.23. The addition of a certain amount of external damping material may be desirable for the purpose of making vibrational power measurements. This is an area for future research.

CHAPTER 6

CONCLUSION

6.1 Loss Factors

The critical frequency of a plate is the frequency at which the bending wave speed is equal to the acoustic wavespeed in the air. Above this frequency the losses are dominated by acoustic damping. The theoretical expression [14] for calculating the critical frequency f_c of a homogeneous plate is

$$f_c = c^2 / (1.8c_L h) \quad (6.1)$$

where c is the wavespeed in the air, c_L is the longitudinal wave velocity in the plate material, and h is the plate thickness. This expression gives a critical frequency of 2000 Hz for the 1/4 in thick plate and of 1000 Hz for the 1/2 in thick plate. These theoretical values correspond well with the peaks obtained in figures 5.3 and 5.4.

The theoretical bending modal density for a plate [14] in units of modes per radian is

$$n = A / (3.6c_L h) \quad (6.2)$$

where A is the surface area of the plate. Based upon this expression, the results in figures 5.3 and 5.4 account for approximately 50% of the bending modes in the 0-4000 Hz frequency range.

For the 1/4 in plate, the loss factors from the energy method were all within 7.% of the average value obtained from the MDOF complex exponential method for each 500 Hz band. For the 1/2 in plate, the loss factors from the energy method were all within 10% of the average value obtained from the MDOF complex exponential method for most of the 500 Hz bands. The exception occurred in the 0-500 Hz band which had a 19% error.

In addition, an attempt was made early in this research to obtain the loss factors through the decay method. The records of the logarithmic energy decays, however, displayed slopes which varied with time. Thus, it was impossible to obtain unambiguous loss factors from the decays. Still, the decays appeared to be dominated by modes with lower damping ratios than can be accounted for by the individual measurements from the complex exponential method. If such modes do exist, it is possible that they were undetectable in the frequency response functions due to overlapping with more highly damped modes. The MDOF complex exponential method would thus tend to overestimate the average loss factor in a band. Nevertheless, the loss factors obtained by the MDOF complex exponential method agreed very well with those obtained by the energy method as shown in figures 5.19 and 5.20.

6.2 Direct and Reverberant Field Considerations

Equation (1.2) is valid provided the velocity is measured in regions of the plate where the reverberant field energy is much greater than the direct field energy. Equations (1.3) and (1.4) were used to check the ratio of the direct field energy density to the reverberant field energy density. These ratios were computed assuming that the boundary loss factors were negligible compared to the distributed loss factors. The radius for these calculations was taken as the average radius of the ten accelerometer locations from the shaker. The ratio for the 1/4 in plate was 0.071 for the 2250 Hz frequency band. This is the band which had the highest average loss factor. In the other bands, the ratios were much smaller. According to this ratio, the reverberant field method should yield a power value 7% higher than the impedance head value for the 2250 Hz band. The reverberant field values were actually an average of 6% less than the corresponding impedance head values for this band. The ratio for the 1/2 in plate was 0.051 for the 1250 Hz band. For this case the reverberant field method yielded power values which were an average of 8%

greater than the corresponding impedance head values. These results indicate that the experimental conditions were acceptable with respect to the reverberant field assumptions.

6.3 Input Power Results

The power input measured by the reverberant field method agreed very well with the measurements obtained from the force and acceleration signals from the impedance head. The results obtained for the 1/4 in plate were generally better than those obtained for the 1/2 in plate. This may be due to the fact that the 1/4 in plate has a modal density which is twice that of the 1/2 in plate. The 1/4 in plate thus has twice as many modes to carry the reverberant energy in each 500 Hz band. Furthermore, the results obtained for each change in the shaker potential verified the linearity of the system over the range tested.

These results have thus provided experimental verification of the reverberant field method and have demonstrated the application of the MDOF complex exponential method to referee structures which have relatively high modal densities. In addition, these results have demonstrated the validity of using the impedance head method to calibrate referee structures in terms of their loss factors.

6.4 Point Impedance

In order to make the reverberant field energy method more practical, though, the plate selected as a referee structure must have the same point impedance characteristics as the structure upon which the vibration source is to be permanently mounted. Thus, an accurate prediction of the point impedance of a referee plate is desirable. Theoretical expressions for the point impedance of infinite plates and other special structures have been derived by Cremer [14].

For an infinite plate, the theoretical point impedance is purely real. For a finite plate with relatively high damping, the theoretical point impedance approaches that of an infinite plate. On the other extreme, a finite plate with no damping has a theoretical point

impedance which is purely imaginary since no steady state power can be injected into the plate. Furthermore, the point impedance of finite plates is affected by the presence of reflected waves. Depending on the coherency of the reverberant and direct fields, the reflected waves might cause the velocity at the injection point to be out of phase with the force input.

Above the critical frequency, the point impedance of the 1/4 in thick plate compared very well with the theoretical value for an infinite plate. Below the critical frequency, however, the point impedance measurements were much lower than the theoretical value. When a layer of external damping material was applied to fully cover one side of the 1/4 in thick plate, the point impedance measurements below the critical frequency improved dramatically; the measurements above the critical frequency remained approximately the same. Thus the addition of external damping material had the effect of reducing the reverberant field strength below the critical frequency.

The 1/2 in thick plate was tested without any external damping material. The real point impedance measurements were well below the theoretical value for an infinite plate. Furthermore, the imaginary point impedance measurements were very high, particularly above the critical frequency. The imaginary components resulted from the relatively low damping and the finite dimensions of the 1/2 in thick plate. Both of these factors resulted in a relatively high reverberant to direct field strength.

The 1/4 in thick plate thus had point impedance values resembling those of an infinite plate. The 1/2 in thick plate had point impedance values which rest somewhere in between the two extreme theoretical cases described above.

6.5 Recommendations

An area in which additional research is needed is the optimum amount of external damping. Adding damping material should have the effect of making the point impedance

of the plates more predictable. Since the damping material would increase the ratio of the distributed loss factor to the boundary loss factor, the effect of minor variations in the boundary conditions would be reduced. But the added damping would also reduce the reverberant to direct field energy density ratio and thus threaten the assumptions made in deriving the reverberant field energy method, equation (1.2). Furthermore, additional damping would cause the modal overlapping to be more severe. The loss factors would thus be more difficult to obtain even with the MDOF complex exponential method. Thus, the trade-offs encountered in adding external damping material need to be explored more fully.

Another area which needs further attention is the mounting of the vibration source to the referee plate. Of course, the device must be mounted to the referee plate in the same fashion that it is to be mounted to the permanent structure. But how sensitive is the power injection to minor differences in mounting?

Furthermore, when a structure undergoes high levels of rotation or transverse response at the device attachment point, the device becomes an active portion of the structure itself. How would this affect the power flow? Would geometrical differences between the referee plate and the permanent structure be an important consideration in this case?

The most difficult part of carrying out the reverberant field energy method is obtaining accurate loss factors. Above the critical frequency, the losses are clearly dominated by acoustic radiation. How would changes in the room air affect this radiation? Acoustic radiation is a function of the characteristic impedance, which varies with temperature. Thus, the change in radiation could be calculated with respect to the change in temperature provided all of the other effects remained the same. But how would changes in humidity affect the radiation?

How does the plate couple with the room space? Does the room feed back energy into the plate? Does the proximity of tables and equipment interfere with the radiation?

In addition, the reverberant field energy method, as considered in this thesis, assumes that the output of the device is in the form of broadband vibrational power. How could this method be applied to the case where the output is in the form of a pure tone? Would it be possible to measure this output if there were modes to carry the energy at the frequency of the tone?

Although this thesis has provided experimental validation of the reverberant field energy method, many questions remain to be answered before this method can be used with confidence in practical situations.

BIBLIOGRAPHY

1. R. Lyon and G. Maidanik 1962 *J. acoust. Soc. Amer.* **34**, 623. Power flow between linearly coupled oscillators.
2. P. Smith 1962 *J. acoust. Soc. Amer.* **34**, 640. Response and radiation of structural modes excited by sound.
3. R. Lyon and P. Smith 1965 *NASA Report, CR- 160*. Sound and structural vibration.
4. R. Lyon 1975 *Statistical Energy Analysis of Dynamical Systems*. Cambridge, Mass.: Massachusetts Institute of Technology Press.
5. B. Clarkson 1981 *European Space Agency Journal*. **5**, 137. Prediction of high-frequency structural vibrations using statistical energy analysis (SEA).
6. B. Clarkson and R. Pope 1981 *J. Sound Vib.* **77**, 535. Experimental determination of modal densities and loss factors of flat plates and cylinders.
7. B. Clarkson and M. Ranky 1983 *J. Sound Vib.* **89**, 309. Frequency average loss factors of plates and shells.
8. B. Clarkson and K. Brown 1984 *Proc. Vibration Damping Workshop*. Wright-Patterson Air Force Base, Ohio. Average Loss Factors for use in Statistical Energy Analysis.
9. E. Dimitriadis 1984 *Thesis, Department of Mechanical Engineering, Georgia Institute of Technology*. Random vibrations of multicomponent structures.
10. C. E. Wallace 1986 *Research paper, SS-3, 112th meeting, Acoustical Society of America*, Anaheim, CA. Diffuse field waves on a thin plate.
11. D. Ewins 1984 *Modal Testing Theory and Practice*. Hertfordshire, England: Research Studies Press Ltd.
12. F. Fahy and R. Pierri 1977 *J. acoust. Soc. Amer.* **62**, 1297. Application of cross-spectral density to a measurement of vibration power flow between connected plates.
13. F. Fahy 1969 *J. Sound Vib.* **10**, 517. Measurement of mechanical input power to a structure.
14. L. Cremer and M. Heckl 1973 *Structure-Borne Sound*. New York: Springer-Verlag.
15. B. Clarkson 1981 *J. Sound Vib.* **77**, 583. The derivation of modal densities from point impedances.
16. S. Crandall 1970 *J. Sound Vib.* **11**, 3. The role of damping in vibration theory.
17. W. Thomson 1981 *Theory of Vibration with Applications*. Englewood Cliffs, N.J.: Prentice-Hall.

APPENDIX A

IMPEDANCE HEAD POWER PROGRAM

The following program was written in Time Series Language (TSL). TSL is a high-level programming language that is specifically designed for signal processing and time series analysis applications. TSL is similar to the BASIC language but is oriented toward the processing of real and complex data arrays, with a large set of "block arithmetic" instructions; including a Fourier transform algorithm and related spectral averaging functions for spectral analysis. The block arithmetic instructions provide for programming of array operations in a single statement, without the complexity of subscripted variables and repetitive loops. TSL also includes commands which set the analog-to-digital converter (ADC) prior to data acquisition.

Program PIH determines the power injection from the force and acceleration signals output by an impedance head according to equation (2.12). This program assumes that the acceleration signal is connected to channel A and the force signal to channel B of the ADC. Comments are included in the following listing for the sake of clarity. Due to memory considerations, however, these comments were not included in the original code.

PROGRAM PIH

C The following lines turn the trigger off, undefine the storage blocks, set the frame size
C to 512, and set the channel code to AB.

```
10 LET I12,0
20 BLKCLR
30 LET I15,512
40 LET I14,3
```

C The program asks the user to input the number of averages.

```
50 PRINT 'INPUT NO. OF AVERAGES'
60 INPUT I5
```

C The following lines set the buffer code to double, the average removal to 0, the zero
C insertion to 0, the error traps to disable, and the Hanning window to off.

```
70 LET I13,1
80 LET I8,0
90 LET I7,0
100 LET I6,0
110 LET I4,0
```

C The maximum voltage input for channels A and B is set at 5 volts.

```
120 LET R13,5
130 LET R12,5
140 BLKDEF B13,26,0
150 ZERO B13
160 BLKDEF B14,30,0
170 ZERO B14
180 LET R2,0
190 FOR I2,0,24
200 SUM B13,I2,B13,I2,R2
210 SUM R2,R2,500
220 NEXT I2
```

C The bandwidth is set to the range 0 - 12800 Hz.

```
230 LET R15,12800
```

C The subsequent operations are performed within subroutines.

```
240 GOSUB 280
250 GOSUB 750
260 GOSUB 870
270 RETURN
```

C The following subroutine controls the analog-to-digital input subsystem by setting
C the sampling frequency, the filter settings, input coupling, etc.

```
280 BLKCLR B0,B1,B5,B6,B8
290 BLKCLR B11,B9,B8
300 STACK GI0,GI1,GI2
310 HLET I0,I14,'XXA B AB'
320 STACK 25000,R15,MIN,PR0
330 ADSET 'SU',B0,I15,I0,R0,R13,'VB',R12
340 HLET I0,I9,'ACDC'
350 HLET I1,I8,'DDED'
360 HLET I2,I7,'DZEZ'
370 ADSET 'CL',I0,I1,I2
380 HLET I0,I6,'ETDT'
390 HLET I1,I13,'SBDB'
400 ADSET I0,I1
410 STACK PI2,PI1,PI0
```

C The following loop begins the actual data acquisition.

```
420 FOR I0,1,I5
430 PROD R7,R15,2
440 ADSET 'SF',R7
450 ADSET 'FA',R15
460 ADSET 'FB',R15
470 ADSET 'SA'
```

C DFT is a TSL command which obtains the Fourier transforms of the force and acceleration signals.

```
480 DFT B0,I4
490 DFT B1,I4
```

C CSPEC is a TSL command which accumulates the cross conjugate products of the force and acceleration signals, the cross-spectrum.

```
500 CSPEC B1,B0,B7
510 NEXT I0
```

C The data acquisition has now ended. CPHASE is a TSL subroutine which compensates phase for sequential sampling of the signals.

```
520 CPHASE B7,1
```

C NORM is a TSL subroutine which normalizes averages to frame count.

```
530 NORM
540 BLKCLR B0,B1
550 MLCONR 1000,B7
```

C The cross-spectrum is divided by 2π .

```
560 MLCONR .1592,B7
```

C The cross-spectrum is multiplied by the transducer calibration factors. This factor must be changed adjusted to the sensitivities of the impedance head transducers.

```
570 MLCONR 4988,B7
580 MLCONR 1000,B7
590 MLCONR 2.,B7
600 BIBSET B7,5,I0
```

C The next lines transform the cross-spectrum into a cross-spectral density.

```
610 QUOT R3,R15,I0
620 PROD R7,R3,.5
630 LET R2,1.
640 BLKDEF B11,I0,0
```



```
650 ZERO B11
660 FOR I2,0,I0
670 PROD R1,R3,I2
680 IF I2,3,690,690,700
690 LET R1,100.
700 LET B11,I2,R1
710 NEXT I2
720 DIV B11,B7
```

C The imaginary component of the cross-spectral density is taken.

```
730 IMAG B7,B9
740 RETURN
750 REMARK
```

C The following subroutine finds the total power for each 500 Hz constant bandwidth.

```
760 FOR I2,0,21
770 LET R9,0.
780 PROD I3,I2,10
790 FOR I4,1,10
800 SUM I3,I3,1
810 LET R10,B9,I3
820 SUM R9,R9,R10
830 NEXT I4
840 LET B14,I2,R9
850 NEXT I2
860 RETURN
```

C The final subroutine prints the power results for each band in units of microwatts:

```
870 FOR I2,0,21
880 LET R1,B14,I2
890 PRINT I2,' ',R1
900 NEXT I2
910 RETURN
END
```

APPENDIX B

MEAN SQUARE VELOCITY PROGRAM

The following program VLX5 was written in the TSL language. This program determines the mean square velocity averaged from a number of locations which the user inputs. The mean square acceleration is measured by an accelerometer. The acceleration auto-spectrum is divided by ω^2 in order to obtain the velocity auto-spectrum. Comments are included in the following listing for the sake of clarity. Due to memory considerations, however, these comments were not included in the original code.

PROGRAM VLX5

C The following lines turn the trigger off, undefine the storage blocks, set the frame size C to 512, and set the channel code to AB.

```
10 LET I12,0
20 BLKCLR
30 LET I15,512
40 LET I14,3
```

C The program asks the user to input the number of averages per accelerometer location.

```
50 PRINT 'INPUT NO. OF AVERAGES'
```

C The following lines set the buffer code to double, the average removal to 0, the zero C insertion to 0, the error traps to disable, and the Hanning window to off.

```
60 INPUT I5
70 LET I13,1
80 LET I8,0
90 LET I7,0
100 LET I6,1
110 LET I4,0
```

C The maximum voltage input for channels A and B is set at 5 volts.

```
120 LET R13,5
130 LET R12,5
140 BLKDEF B13,26,0
150 ZERO B13
160 BLKDEF B14,30,0
```

```

170 ZERO B14
180 LET R2,0
190 FOR I2,0,24
200 SUM B13,I2,B13,I2,R2
210 SUM R2,R2,500.
220 NEXT I2

```

C The bandwidth is set to the range 0 - 12800 Hz.

```

230 LET R15,12800.

```

C The subsequent operations are performed within subroutines.

```

240 GOSUB 370
250 FOR I11,0,24
260 LET R11,B13,I11
270 GOSUB 950
280 NEXT I11
290 FOR I2,0,23
300 GOSUB 340
310 NEXT I2
320 GOSUB 1040
330 RETURN
340 SUM I3,I2,1
350 DIF B14,I2,B14,I3,B14,I2
360 RETURN

```

C The following subroutine controls the analog-to-digital input subsystem by setting the sampling frequency, the filter settings, input coupling, etc.

```

370 BLKCLR B0,B1,B5,B6,B8
380 BLKCLR B11,B9,B8
390 STACK GI0,GI1,GI2
400 HLET I0,I14,'XXA B AB'
410 STACK 25000.,R15,MIN,PRO
420 ADSET 'SU',B0,I15,I0,R0,R13,'VB',R12
430 HLET I0,I9,'ACDC'
440 HLET I1,I8,'DDED'
450 HLET I2,I7,'DZEZ'
460 ADSET 'CL',I0,I1,I2
470 HLET I0,I6,'ETDT'
480 HLET I1,I13,'SBDB'
490 ADSET I0,I1
500 STACK PI2,PI1,PI0

```

C The user inputs the number of accelerometer locations to be used.

```

510 PRINT 'INPUT NO. OF LOCATIONS'
520 INPUT I1

```

C The next two loops begin the actual data acquisition.

```

530 FOR I11,1,I1
540 FOR I0,1,I5
550 PROD R7,R15,2.
560 ADSET 'SF',R7
570 ADSET 'FA',R15
580 ADSET 'FB',R15
590 ADSET 'SA'

```

C DFT is a TSL command which obtains the Fourier transform of the acceleration signal.

```
600 DFT B0,I4
```

C ASPEC is a TSL command which obtains the auto-spectrum of the Fourier transform
C of the acceleration.

```

610 ASPEC B0,B7
620 NEXT I0
630 IF I11,I1,640,660,660

```

C The user is instructed to move the accelerometer. The user may press any number key
C to continue the averaging.

```

640 PRINT 'MOVE ACCELEROMETER'
650 INPUT R2
660 LET R2,0.
670 NEXT I11
680 PROD I5,I5,I1

```

C The data acquisition has now ended. NORM is a TSL subroutine which normalizes the
C averages to the frame count.

```

690 NORM
700 BLKCLR B0,B1
710 MLCONR 1000.,B7

```

C The next two lines divide the auto-spectrum by $4\pi^2$.

```

720 MLCONR .1592,B7
730 MLCONR .1592,B7

```

C The accelerometer calibration factor is supplied in the next two lines.

```

740 MLCONR 1080.,B7
750 MLCONR 1080.,B7
770 MLCONR 1000.,B7
775 MLCONR 2.,B7

```

C The following group of lines divide the auto-spectrum by the frequency squared.

```

780 BIBSET B7,5,I0
790 QUOT R3,R15,I0
800 PROD R7,R3,.5
810 LET R2,1.
820 BLKDEF B11,I0,0
830 ZERO B11
840 FOR I2,0,I0
850 PROD R1,R3,I2
860 IF I2,1,870,880,880
870 LET R1,1000.
880 PROD R1,R1,R1
890 LET B11,I2,R1
900 NEXT I2
910 DIV B11,B7
920 MOVE B7,B9
930 INTG B9
940 RETURN
950 REMARK

```

C The following subroutine finds the total mean square velocity for each 500 Hz
 C constant bandwidth.

```

960 FOR I2,0,I0
970 PROD R1,R3,I2
980 IF R1,R11,1020,990,990
990 LET B14,I11,B9,I2
1000 SUM I3,I11,1
1010 LET I2,10000.
1020 NEXT I2
1030 RETURN

```

C The final subroutine prints the mean square velocity for each band in units of
 C $10^6 * (m / sec)^2$.

```

1040 FOR I2,0,21
1050 LET R1,B14,I2
1060 PRINT I2,'      ',R1
1070 NEXT I2
1080 RETURN
END

```

APPENDIX C

POINT IMPEDANCE PROGRAM

The following program TMM was written in the TSL language. This program determines the point impedance from the force and acceleration signals output by the impedance head transducer. The program assumes that the acceleration signal is connected to channel A and the force signal to channel B of the ADC. Comments are included in the following listing for the sake of clarity. Due to memory considerations, however, these comments were not included in the original code.

PROGRAM TMM

C The following lines turn the trigger off, undefine the storage blocks, set the frame size
C to 1024, and set the channel code to AB.

```
10 LET I12,0
20 BLKCLR
30 LET I15,1024
40 LET I14,3
```

C The program asks the user to input the number of averages.

```
50 PRINT 'INPUT NO. OF AVERAGES'
55 INPUT I5
```

C The following lines set the buffer code to double, the average removal to 0, the zero
C insertion to 0, the error traps to disable, and the Hanning window to off.

```
60 LET I13,1
70 LET I8,0
80 LET I7,0
90 LET I6,1
100 LET I4,0
```

C The maximum voltage input for channels A and B is set at 5 volts.

```
110 LET R13,5
120 LET R12,5
130 BLKDEF B13,26,0
140 ZERO B13
150 BLKDEF B14,30,2
```

```

160 ZERO B14
170 LET R2,0
180 FOR I2,0,8
190 SUM B13,I2,B13,I2,R2
200 SUM R2,R2,500.
210 NEXT I2

```

C The bandwidth is set to the range 0 - 12800 Hz.

```

220 LET R15,12800.

```

C The subsequent operations are performed within subroutines.

```

230 GOSUB 370
240 FOR I11,0,24
250 LET R11,B13,I11
260 GOSUB 830
270 NEXT I11
280 FOR I2,0,8
290 GOSUB 330
300 NEXT I2
310 GOSUB 940
320 RETURN
330 SUM I3,I2,1
340 DIF B14,I2,B14,I3,B14,I2
350 LET C14,B14,I2
360 RETURN

```

C The following subroutine controls the analog-to-digital input subsystem by setting the
C sampling frequency, the filter settings, input coupling, etc.

```

370 BLKCLR B0,B1,B5,B6,B8
380 BLKCLR B11
390 STACK GI0,GI1,GI2
400 HLET I0,I14,'XXA B AB'
410 STACK 25000.,R15,MIN,PRO
420 ADSET 'SU',B0,I15,I0,R0,R13,'VB',R12
430 HLET I0,I9,'ACDC'
440 HLET I1,I8,'DDED'
450 HLET I2,I7,'DZEZ'
460 ADSET 'CL',I0,I1,I2
470 HLET I0,I6,'ETDT'
480 HLET I1,I13,'SBDB'
490 ADSET I0,I1
500 STACK PI2,PI1,PI0

```

C The following loop begins the actual data acquisition.

```

510 FOR I0,1,I5
520 PROD R7,R15,2.
530 ADSET 'SF',R7

```

```

540 ADSET 'FA',R15
550 ADSET 'FB',R15
560 ADSET 'SA'

```

C DFT is a TSL command which obtains the Fourier transform of the force and
C acceleration signals.

```

570 DFT B0,I4
580 DFT B1,I4

```

C CSPEC is a TSL command which accumulates the cross-conjugate products of
C the force and acceleration signals, the cross-spectrum.

```

590 CSPEC B0,B1,B8

```

C ASPEC is a TSL command which accumulates the auto-spectrum of the acceleration.

```

600 ASPEC B0,B5
610 NEXT I0
620 BLKCLR B0,B1

```

C The data acquisition is now complete. CPHASE is a TSL subroutine which
C compensates phase for sequential sampling of the signals.

```

630 CPHASE B8,1
640 BIBSET B8,5,I0

```

C The cross-spectrum is multiplied by the transducer calibration factor.

```

650 MLCONR .4355,B8

```

C The cross-spectrum is multiplied by 2π .

```

660 MLCONR 6.283,B8

```

C The cross-spectrum is multiplied by j.

```

670 MLCONC (0.,1),B8

```

C The following group of lines multiply the cross-spectrum by the frequency.

```

680 QUOT R3,R15,I0
690 PROD R7,R3,.5
700 LET R2,1
710 BLKDEF B11,I0,0
720 ZERO B11
730 LET R9,5.
740 FOR I2,0,I0
750 PROD R1,R3,I2
760 SUM B11,I2,B11,I2,R1
770 NEXT I2

```



```
780 MUL B11,B8
```

C The cross-spectrum is divided by the auto-spectrum in order to obtain the point
C impedance.

```
790 DIV B5,B8
800 INTG B8
810 MLCONR R3,B8
820 RETURN
```

C The following subroutine determines the point impedance for each 500 Hz constant
C Bandwidth.

```
830 LET C2,B8,28
840 LET C3,B8,20
850 FOR I2,0,I0
860 PROD R1,R3,I2
870 IF R1,R11,920,880,880
880 SUM B14,I11,B14,I11,B8,I2
890 LET C13,B14,I11
900 SUM I3,I11,1
910 LET I2,10000.
920 NEXT I2
930 RETURN
```

C The final subroutine prints the real and imaginary components of the point impedance
C for each band in units of N sec/m.

```
940 MLCONR .002,B14
950 FOR I2,0,7
960 LET C1,B14,I2
970 PRINT I2,'      ',C1
980 NEXT I2
981 LET B14,22,C8
990 RETURN
END
```

APPENDIX D

DERIVATION OF THE MDOF COMPLEX EXPONENTIAL METHOD

The mathematics of the MDOF complex exponential method are given in this appendix. The starting point is the expression for the receptance frequency response function for a general MDOF system with viscous damping. For a force applied at point k and a displacement at point i, this transfer function is approximated using N modes as

$$H_{ik}(s) = \frac{X_i}{F_k}(s) = \sum_{r=1}^N \frac{A_{ik}^r}{s - s_r} + \frac{A_{ik}^{r*}}{s - s_r^*} \quad (D.1)$$

where

$$s_r = \sigma_r + j\omega_{r,d} = -\zeta_r \omega_r + j\omega_r \sqrt{1 - \zeta_r^2}$$

and * denotes complex conjugate. Now let

$$A_{r+1} = A_r^*$$

$$s_{r+1} = s_r^*$$

$$r = 1, 3, 5, 7, \dots$$

The transfer function (D.1) can thus be written as

$$H(s) = \frac{X}{F}(s) = \sum_{r=1}^{2N} \frac{A_r}{s - s_r} \quad (D.2)$$

where the subscripts i and k have been omitted for convenience. Thus, $2N$ is the number of degrees of freedom of the system's model, constituting N conjugate pairs of modes. The corresponding unit impulse response function can be obtained by taking the inverse Fourier transform of the transfer function

$$X(t) = \sum_{r=1}^{2N} A_r \exp[s_r t] \quad (D.3)$$

If the original frequency response function is obtained in digital form and is thus desrobed at each of a number of equally-spaced frequencies, the resulting inverse response function will be similarly described at a corresponding number of equally-spaced time intervals. Thus let the time interval from t_0 to t_{2N} be divided into $2N$ equal subintervals. The value of $X(t)$ for the K th subinterval is

$$X(t_K) = \sum_{r=1}^{2N} A_r \exp[s_r K T] \quad (D.4)$$

where

$$K = 0, 1, 2, \dots, 2N$$

$$T = \text{value of the time subinterval}$$

Now let $U_r = \exp[s_r T]$. Equation (D.4) can thus be written as

$$X(t_K) = \sum_{r=1}^{2N} A_r U_r^K \quad (D.5)$$

The full set of K samples is thus

$$\begin{aligned}
X(t_0) &= A_1 + A_2 + A_3 + \dots + A_{2N} \\
X(t_1) &= A_1 U_1 + A_2 U_2 + \dots + A_{2N} U_{2N} \\
X(t_2) &= A_1 U_1^2 + A_2 U_2^2 + \dots + A_{2N} U_{2N}^2 \quad (D.6)
\end{aligned}$$

$$\begin{aligned}
&\cdot \qquad \qquad \qquad \cdot \\
&\cdot \qquad \qquad \qquad \cdot \\
&\cdot \qquad \qquad \qquad \cdot
\end{aligned}$$

$$\begin{aligned}
X(t_{2n-1}) &= A_1 U_1^{2n-1} + A_2 U_2^{2n-1} + \dots + A_{2N} U_{2N}^{2n-1} \\
X(t_{2n}) &= A_1 U_1^{2n} + A_2 U_2^{2n} + \dots + A_{2N} U_{2N}^{2n}
\end{aligned}$$

If the number of data points n is equal to the number of modes N , there will be $2n+1$ rows for equation (D.6). Now taking equation (D.6), multiply row 1 by a_{2n} , row 2 by a_{2n-1} , and so on, row $2n$ by a_1 , and finally row $2n+1$ by a_0 . Equation (D.6) becomes

$$\begin{aligned}
a_{2n} X(t_0) &= a_{2n} (A_1 + A_2 + \dots + A_{2n}) \\
a_{2n-1} X(t_1) &= a_{2n-1} (A_1 U_1 + A_2 U_2 + \dots + A_{2n} U_{2n}) \quad (D.7)
\end{aligned}$$

$$\begin{aligned}
&\cdot \qquad \qquad \qquad \cdot \\
&\cdot \qquad \qquad \qquad \cdot \\
&\cdot \qquad \qquad \qquad \cdot
\end{aligned}$$

$$\begin{aligned}
a_1 X(t_{2n-1}) &= a_1 (A_1 U_1^{2n-1} + A_2 U_2^{2n-1} + \dots + A_{2n} U_{2n}^{2n-1}) \\
a_0 X(t_{2n}) &= a_0 (A_1 U_1^{2n} + A_2 U_2^{2n} + \dots + A_{2n} U_{2n}^{2n})
\end{aligned}$$

Adding these equations gives

$$\sum_{K=0}^{2n} a_{2n-K} X(t_K) = \sum_{K=0}^{2n} a_{2n-K} \left[\sum_{r=1}^n A_r U_r^K \right] = \sum_{r=1}^n A_r \left[\sum_{K=0}^{2n} a_{2n-K} U_r^K \right] \quad (D.8)$$

The coefficients a_1, a_2, \dots, a_{2n} are taken to be the coefficients in the equation

$$U^{2n} + a_1 U^{2n-1} + a_2 U^{2n-2} + \dots + a_{2n-1} U + a_{2n} = 0 \quad (D.9)$$

for which the roots are U_1, U_2, \dots, U_{2n} . Also note that $a_0 = 1$. The coefficients are sought in order to determine the roots of equation (D.9) and hence the system natural frequencies. Equation (D.9) can be written as

$$\sum_{K=0}^{2n} a_{2n-K} U_r^K = 0 \quad (D.10)$$

since U_r is a root of the polynomial.

Substituting (D.10) into (D.8) yields

$$\sum_{K=0}^{2n} a_{2n-K} X(t_K) = 0 \quad (D.11)$$

An additional $2n - 1$ equations can be obtained by performing the same operation starting with the second row of equation (D.6) and so on. An additional row must be added to equation (D.6) at the start of each repetition. The significance of these operations is to increase t_0 and t_{2n} by T and thus make the final sum invariant. The result is thus

$$\begin{bmatrix} X(t_{2n-1}) & X(t_{2n-2}) & \dots & X(t_0) \\ X(t_{2n}) & X(t_{2n-1}) & \dots & X(t_1) \\ \cdot & \cdot & & \cdot \\ \cdot & \cdot & & \cdot \\ \cdot & \cdot & & \cdot \\ X(t_{4n-2}) & X(t_{4n-3}) & \dots & X(t_{2n-1}) \end{bmatrix} \begin{bmatrix} a_1 \\ a_2 \\ \cdot \\ \cdot \\ \cdot \\ a_{2n} \end{bmatrix} = - \begin{bmatrix} X(t_{2n}) \\ X(t_{2n+1}) \\ \cdot \\ \cdot \\ \cdot \\ X(t_{4n-1}) \end{bmatrix} \quad (D.12)$$

Recall that $X(t_m)$ represents the impulse response function at time t_m . Thus, the data points in each successive row in equation (D.12) overlaps all but one of the data points in the previous row. Equation (D.12) can be solved for a_1, a_2, \dots, a_{2n} . These coefficients can then be substituted into equation (D.9) in order to determine the roots, U_1, U_2, \dots, U_{2n} . The natural frequency ω_r and the damping ratio ζ_r of mode r can then be found as follows,

$$U_r = \exp[s_r T] = \exp[(\sigma_r + j\omega_{r,d})T] = \exp[\sigma_r T] \exp[j\omega_{r,d} T] \quad (D.13)$$

In terms of amplitude and phase angle,

$$|U_r| = \exp[\sigma_r T] \quad (D.14)$$

and

$$\angle U_r = \omega_{r,d} T \quad (D.15)$$

Thus,

$$\frac{\ln |U_r|}{T} = \sigma_r = \zeta_r \omega_r \quad (D.16)$$

and

$$\frac{\angle U_r}{T} = \omega_{r,d} = \omega_r \sqrt{1 - \zeta_r^2} \quad (D.17)$$

The solution may now be completed by deriving the corresponding modal constants, A_1, A_2, \dots, A_{2n} , from equation (D.6). This may be written as

$$\begin{bmatrix} 1 & 1 & 1 & \dots & 1 \\ U_1 & U_2 & U_3 & \dots & U_{2n} \\ U_1^2 & U_2^2 & U_3^2 & \dots & U_{2n}^2 \\ \cdot & \cdot & \cdot & & \cdot \\ \cdot & \cdot & \cdot & & \cdot \\ \cdot & \cdot & \cdot & & \cdot \\ U_1^{2n-1} & U_2^{2n-1} & U_3^{2n-1} & \dots & U_{2n}^{2n-1} \end{bmatrix} \begin{bmatrix} A_1 \\ A_2 \\ A_3 \\ \cdot \\ \cdot \\ \cdot \\ A_{2n} \end{bmatrix} = \begin{bmatrix} X(t_0) \\ X(t_1) \\ X(t_2) \\ \cdot \\ \cdot \\ \cdot \\ X(t_{2n-1}) \end{bmatrix} \quad (D.18)$$

BIOGRAPHICAL SKETCH

Thomas Grant Irvine is the son of John and Sharon Irvine. He was born on January 24, 1961, in Phoenix, Arizona. He received his elementary education at Supai Elementary School in Scottsdale. He completed his secondary education at McClintock High School in Tempe.

In August 1979, he entered the engineering science program at Arizona State University. He received an Arizona Regents Scholarship and a Signal Companies Scholarship. From June 1980 to June 1982, he served as a missionary for the Church of Jesus Christ of Latter-day Saints in Hiroshima, Japan. He subsequently resumed his studies at Arizona State University and received his Bachelor of Science in Engineering degree in May 1985.

During the summers of 1984 and 1985, he worked as an engineering aide at Garrett Turbine Engine Company in Phoenix. In August 1985, he began his graduate studies at Arizona State University, where he worked as a research and teaching assistant in the Department of Mechanical and Aerospace Engineering. He presented the results of his thesis research to the 112th meeting of the Acoustical Society of America in Anaheim, California, on December 11, 1986.